



**Joaquín Antonio CORNEJO JIMENEZ**

Master of Micro and Nanotechnologies for Integrated Systems  
2019-2020

IBM RESEARCH ZURICH  
Säumerstrasse 4, 8803 Rüschlikon, Switzerland

**Study of the process of fabrication of  $VO_2$  devices for application  
on Oscillatory Neural Networks**

from 17/02/2020 to 14/08/2020

Confidentiality: no

Under the supervision of:

**-Company supervisor: Siegfried KARG, [sfk@zurich.ibm.com](mailto:sfk@zurich.ibm.com)**

Present at the defense: yes

**-Phelma tutor: Liliana PREJBEANU, [liliana.buda@cea.fr](mailto:liliana.buda@cea.fr)**

Ecole nationale  
supérieure de physique,  
électronique, matériaux

**Phelma**

Bât. Grenoble INP - Minatec  
3 Parvis Louis Néel - CS 50257  
F-38016 Grenoble Cedex 01

Tél +33 (0)4 56 52 91 00

Fax +33 (0)4 56 52 91 03

**<http://phelma.grenoble-inp.fr>**

**Abstract [EN]:** For almost half a century vanadium oxide compounds have been an object of interest to the scientific community for their very fast metal to insulator transition behavior, with a special focus on  $VO_2$  for its near room temperature phase transition. Devices made with this material have been studied for the fabrication of oscillators to be used in oscillatory neural networks that are able to solve complex tasks on unstructured data such as image recognition. In this thesis we offer a study of the process of fabrication of such a compound using a novel technique of flash anneal on different thicknesses of ALD deposited amorphous vanadium oxide. An additional study of this fast anneal technique on PLD deposited and Ge doped vanadium dioxide was done. A study of different device architectures has been made, comparing a 2D planar architecture and a 3D crossbar architecture. Finally, we offer a few macroscopical models to understand better the working principle of these devices. All of this is done on  $SiO_2$ -on-Si wafers to prepare a process that is compatible with the current CMOS technology.

**Abstrait [FR]:** Depuis près d'un demi-siècle, les composés d'oxyde de vanadium sont un objet d'intérêt pour la communauté scientifique en raison de leur comportement de transition rapide entre des phases métallique et isolante, avec un accent particulier sur le composé  $VO_2$  pour sa transition de phase à température proche de la température ambiante. Les dispositifs fabriqués avec ce matériau ont été étudiés pour la fabrication d'oscillateurs destinés à être utilisés dans des réseaux neuronaux oscillatoires capables de résoudre des tâches complexes sur des données non structurées telles que la reconnaissance d'images. Dans cette thèse, nous proposons une étude du processus de fabrication d'un tel composé en utilisant une nouvelle technique de *flash anneal* sur différentes épaisseurs d'oxyde de vanadium amorphe déposé par ALD. Une étude supplémentaire de cette technique de recuit rapide sur du dioxyde de vanadium déposé par PLD et dopé au Ge a été réalisée. Une étude de différentes architectures de dispositifs a été réalisée, comparant une architecture plane en 2D et une architecture transversale en 3D. Enfin, nous proposons quelques modèles macroscopiques pour mieux comprendre le principe de fonctionnement de ces dispositifs. Tout cela est réalisé sur des wafers de  $SiO_2$ -on-Si afin de préparer un processus compatible avec la technologie CMOS actuelle.

**Astratto [IT]:** Per quasi mezzo secolo i composti di ossido di vanadio sono stati oggetto di interesse da parte della comunità scientifica per il loro comportamento di transizione metallo-isolante molto veloce, con una particolare attenzione a  $VO_2$  per la sua transizione di fase a temperatura ambiente. I dispositivi realizzati con questo materiale sono stati studiati per la fabbricazione di oscillatori da utilizzare nelle reti neurali oscillatorie, che sono in grado di risolvere compiti complessi su dati non strutturati come il riconoscimento di immagini. In questa tesi offriamo uno studio del processo di fabbricazione di tale composto utilizzando una nuova tecnica di flash anneal su diversi spessori di ossido di vanadio depositato via ALD. Uno studio addizionale della tecnica di flash anneal è stato fatto per diossido di vanadio depositato via PLD e Ge drogato. Diverse architetture di dispositivi sono state studiate, confrontando un'architettura planare 2D e una traversa 3D. Infine, offriamo alcuni modelli macroscopici per comprendere meglio il principio di funzionamento di questi dispositivi. Tutto questo viene fatto su wafer  $SiO_2$ -on-Si per preparare un processo compatibile con l'attuale tecnologia CMOS.

## **Acknowledgement**

I would like to thank Dr. Sigfried Karg and Elisabetta Corti for giving me the opportunity to work in such a passionate and fun subject in such an important company that is IBM. I would also like to thank them for the help they provided during the whole of this thesis as well as their constant guidance. I would also like to acknowledge and thank the help given by master student, Federico Balduini, specially for the theoretical framework. Finally I would like to thank Dr. Kirsten Moselund and the whole Materials Integration and Nanoscale Devices group, in which this thesis was done, for letting me be part of such an incredible research environment.

# Contents

<b>1</b>	<b>Introduction</b>	<b>1</b>
<b>2</b>	<b>Context and State of the Art</b>	<b>1</b>
2.1	Vanadium Dioxide: Generalities . . . . .	1
2.2	The Switching Mechanics . . . . .	2
2.3	Process of Fabrication . . . . .	3
2.4	The Devices . . . . .	4
2.5	Oscillatory Neural Networks . . . . .	5
<b>3</b>	<b>Motivation and Objectives</b>	<b>6</b>
<b>4</b>	<b><math>VO_2</math> Thin films</b>	<b>7</b>
4.1	Introduction . . . . .	7
4.2	Results . . . . .	10
4.2.1	Ozone and Oxygen Plasma based process . . . . .	10
4.2.2	Water based process . . . . .	13
4.2.3	Ge doped $VO_2$ . . . . .	20
4.3	Conclusion . . . . .	21
<b>5</b>	<b><math>VO_2</math> Devices</b>	<b>22</b>
5.1	Introduction . . . . .	22
5.2	Results . . . . .	23
5.2.1	Planar Design . . . . .	23
5.2.2	Crossbar Design . . . . .	24
5.2.3	Singular Grain . . . . .	27
5.3	Conclusion . . . . .	30
<b>6</b>	<b>Simulation and Models</b>	<b>31</b>
6.0.1	Conduction Model: Smooth Films . . . . .	31
6.0.2	Simulation: Granular Devices . . . . .	32
<b>7</b>	<b>Conclusion</b>	<b>37</b>
	<b>References</b>	<b>38</b>

## Glossary

**ALD** Atomic Layer Deposition.

**FA** Flash Lamp Anneal.

**ICP** Inductively Coupled Plasma.

**IMT** Insulator-to-Metal Transition.

**MIT** Metal-to-Insulator Transition.

**ONN** Oscillatory Neural Networks.

**PLD** Pulsed Laser Deposition .

**SThM** Scanning Thermal Microscope.

**TEC** Temperature control system.

**TEMAV** Tetrakis[ethylmethylamino]vanadium (Vanadium source).

**UCAM** University of Cambridge.

# 1 Introduction

During the past century machine learning has been getting traction on the scientific community for its capabilities for solving problems of high complexity based on unstructured data.

These algorithms currently run on traditional platforms, based on the Von Neuman processor architecture. In these types of processor, the speed and the power efficiency of machine learning algorithm is limited by the so-called "Von Neumann bottleneck", caused by the physical separation of the processing unit from the memory. As time has gone by processing units or CPUs have become faster and faster as memories have, but the maximum data transfer rate between each other has stayed the same. Therefore, the CPU is often forced to wait for the data transfer from the memory units causing a higher latency and an unnecessary consumption of power. It is of great interest for technologist to find a replacement of this architecture that circumvents this problem and that acts as an accelerator of machine learning programs.

The brain has always been a computing element whose capabilities and properties have baffled scientists for a really long time. It is organized in full three dimensional way, it is self learning, it is robust and power efficient, and one can think of many more things that makes the brain arguably better than current computers in dealing with complex tasks as image recognition. So it is not a surprise that scientist are now trying to find inspiration mimicking nature's way of doing things. Neural networks have been one of the first results of this biomimetic approach. The logical step forward would be to implement their architecture in hardware, for example exploiting the concept of "in memory computing", therefore bringing the computation directly next to the memory units.

As a possible implementation, it has been shown that systems of coupled oscillators can form neural networks, called oscillatory neural network (ONN), that can perform tasks as image recognition exploiting their associative memory capabilities. As put simply by the Russian mathematician Eugene M. Izhikevich: "*anything that can oscillate can also compute*" [1].

Following this paradigm oscillatory systems have been devised to make this possible [2]. Oscillatory neural networks offer also other "extra" advantages against traditional digital approaches, like resilience to noise, they can be easily read out with standard electronics, they are energy efficient, etc...

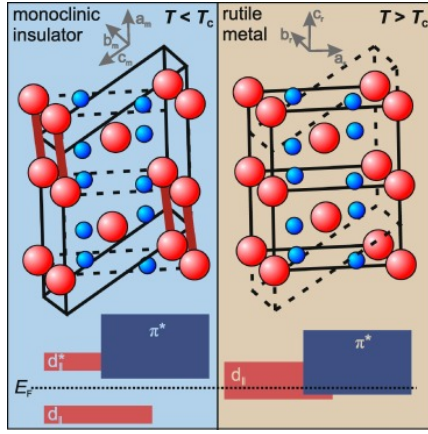
Finally, one possibility to make very compact oscillators is with  $VO_2$  oscillators.  $VO_2$  is a material that has an abrupt phase transition near room temperature and that by applying a DC voltage can be easily used to create high frequency oscillators. It has been shown that these oscillators can be coupled through resistive or capacitive elements between each other [3] and they can behave as a complete neural network where the information is encoded in the time domain.

## 2 Context and State of the Art

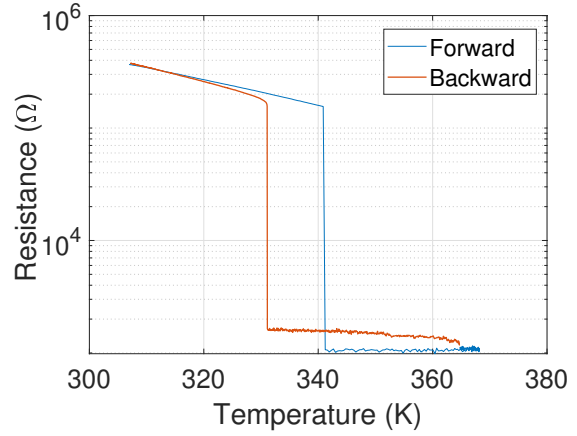
This section is dedicated to the presentation of the preliminary information that the reader needs, to understand the context in which this thesis has been done. It is also to define the state of the art from where this thesis proceeds.

### 2.1 Vanadium Dioxide: Generalities

Vanadium oxide systems have been of great interest for their phase switching properties, i.e. their capability of changing their resistivity from insulating to metallic when heated. They exist in many different compounds such as  $VO_2$ ,  $V_2O_5$ ,  $V_6O_{13}$ , etc... The  $VO_2$  compound is considered to be of special interest because its transition temperature is close to room temperature. This material has two meta stable structural phases with different physical properties. The monoclinic insulating phase (M1) is a high resistivity phase, and it is present at ambient temperatures, the tetragonal rutile metallic phase (R) has a low resistivity, and is present at higher temperatures (see figure 1). The transition between this two phases, also known as Metallic to Insulator transition (MIT) or Insulator to Metal transition (IMT), depending on the direction of the transition, happens at a temperature of about 340 K (see figure 1b for an example of resistivity vs temperature). In literature it has been reported that this phase change can go as far as five order of magnitude of resistance change from one state to another at a very high speed (about 10ns [7]) for a monocrystalline material [15].



(a) Different phases corresponding to  $VO_2$ [8]



(b) Resistance vs temperature sweep example.

Figure 1: Vanadium dioxide phase change.

## 2.2 The Switching Mechanics

During the '50s the switching property of the material was first observed by Morin [14]. But the exact process that regulates the transition is not yet well understood and it is a subject of debate in the scientific community. There are two schools of thought: the temperature caused transition by phonon-electron interaction called Peierls Transition, the electric field caused transition by electron-electron interaction called Mott-Hubbard or just Mott transition.

To give a short overview, the Peierls transition mechanism is usually a mechanism that happens in one dimensional chain of equally spaced conductors, that undergo a change in the periodicity of the chain as shown in figure 2.

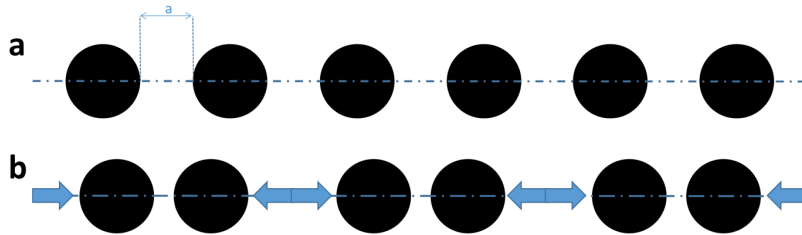


Figure 2: Change of periodicity in a 1D-chain of conductors where **a** is the conducting chain and **b** is the chain after a transition, in an insulating state.

The change of the periodicity in the system creates band gaps near the edge of the Brillouin zone as shown in figure 3.

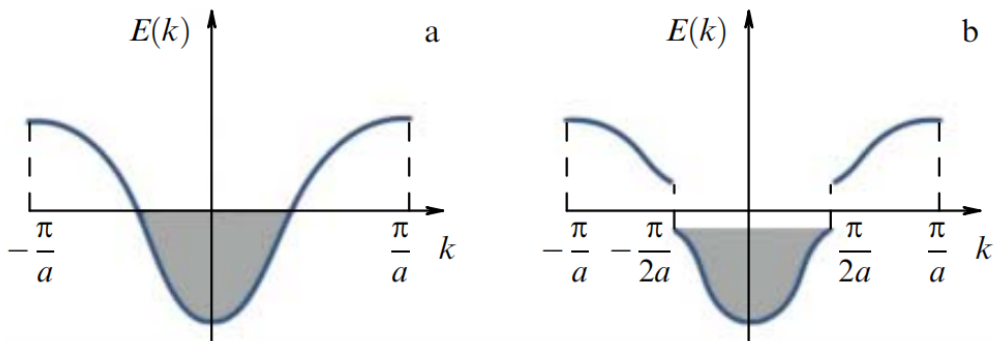


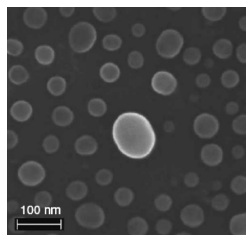
Figure 3: Energy bands of a 1D chain before (a) and after (b) the change of periodicity. [9]

In the '70s John B. Goodenough [10] was able to prove that even if the material was not a one dimensional chain, the  $VO_2$  band gap was due to a pairing between the vanadium atoms in a 1D-like chain. This claim was supported by other authors [11, 12]. This projected the Peierls mechanism as the main explanation of this phenomena. However there are still some points that this mechanism by itself cannot justify, for instance, the "[.] band gap of 0.6 eV for the M1 phase, the appearance of the M2 phase (which is another insulating phase present in this material at lower temperatures)[..and other..] magnetic features of the MIT" as was pointed out by Shao et al. in [13]. Researchers therefore often mention that a Mott-Hubbard mechanism accompanies this phenomena. The Mott-Hubbard transition is mostly related to Coulombic repulsion between the electrons inside of the material. This model proposes that the transition happens when the carrier density reaches a critical value, this value is defined by equation  $n_c^{1/3} a_H \approx 0.2$  where  $n_c$  is the critical carrier density defined by the material and  $a_H$  is the Bohr radius. Once the carrier density is bigger than this value electron-electron correlation is strong enough to cause the transition to the material's metallic phase.

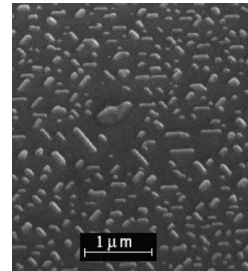
These two phenomena have been proposed as the origin of the MIT in  $VO_2$ . Which one is the main mechanism and which one is secondary it is not yet clear. However many times it has been shown that, even if voltage/current triggering is used at constant temperature to try to activate the Mott-Hubbard transition, this triggering can be mainly attributed to joule self heating inside of the material and therefore to the Peierls mechanism [25, 26, 27].

### 2.3 Process of Fabrication

The fabrication of films of  $VO_2$  is generally done by a deposition of amorphous vanadium oxide followed by an annealing step to get the right stoichiometry [16, 18, 20]. It has been shown that the fabrication of  $VO_2$  thin films on Si substrates causes the material to be granular because of high lattice mismatch [16]. The fabrication of  $VO_2$  films on Si substrates remains of great interest for compatibility with already existent CMOS processes. For a better lattice matching  $Al_2O_3$  (Sapphire) [16] or  $TiO_2$  [28] substrates are often used. On these substrates the growth of  $VO_2$  crystals produces monocrystalline rods, which would make the fabrication of single crystal devices possible. The issue lies in the fact that these kinds of substrates are significantly more expensive than a common Si-wafer and makes the CMOS compatibility difficult. Another interesting point of using matched-lattice substrates is that it is possible to enhance or even change the switching properties of  $VO_2$  through intrinsic stress because of the low but still existing lattice mismatch [28]. Another way that is used to tune the switching temperature is through doping materials, like germanium for instance. It has been shown that germanium doped  $VO_2$  can have a higher temperature of IMT [17].



(a)  $VO_2$  growth in Si substrate.



(b)  $VO_2$  growth in  $Al_2O_3$  substrate.

Figure 4: SEM images of  $VO_2$  growth in two different substrates. (S.A.Pauli et. al[16])

In figure 4 some examples are shown of what is the result of growing  $VO_2$  in different substrates, comparing growth in Si substrates and Sapphire substrates.

For the deposition various methods are found to be used in the literature: Pulsed Laser Deposition (PLD) [16, 18], reactive magnetron sputtering [20] or Atomic Layer Deposition (ALD) [24, 30, 31], to name a few. In a previews paper done by our team comparing PLD fabricated devices and ALD fabricated devices it was shown that the ALD process was more suitable for our purposes due to reduced variability between devices [19]. For this reason ALD of  $VO_x$  is the deposition technique explored and optimized in the course of this thesis. We will be using tetrakis[ethylmethylamino]vanadium (or TEMAV) as a precursor for vanadium and will explore oxygen plasma, ozone and water [30, 31, 32] as a precursor for oxygen. For the annealing generally the classic "slow" annealing techniques are used. In general after the annealing there is a certain material "path" that vanadium oxide follows. Upon the increase

of temperature of oxygen partial pressure in the chamber, the deposited amorphous oxide will transform into the  $VO_2$  compound with an increasing quality, after determined values of temperature and/or oxygen partial pressure an increasing quantity of  $V_2O_5$  contaminations is measured on the  $VO_2$  layer. Finally at high temperatures and pressures, the  $VO_2$  compound will completely transform into its more stable counterpart  $V_2O_5$  [36].

There is no report to our knowledge of fast annealing techniques, like flash lamp anneal, being used for the fabrication of  $VO_2$ . The exploration of the previously mentioned technique will be discussed in the following chapters of this thesis.

## 2.4 The Devices

After deposition and annealing,  $VO_2$  films are patterned with Inductively Coupled Plasma (ICP) etching and contacted with nickel/gold electrodes. In the scope of this thesis the films are patterned in two different configurations: planar 2D devices [19, 21, 22] or crossbar [23] 3D devices, which are displayed in figure 5.

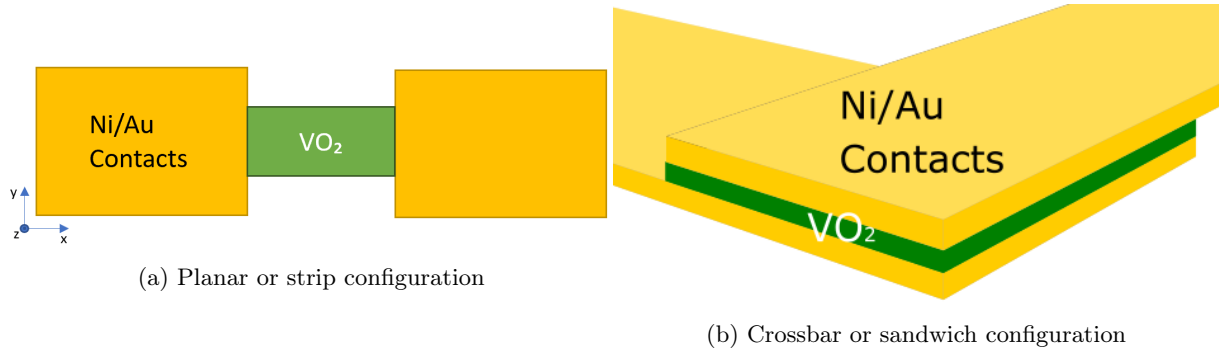


Figure 5: Schematics of the two device configuration.

It has been shown previously by simulation that it is possible to use such elements to create a network that effectively does pattern recognition[19]. The system is composed of  $VO_2$  based oscillators. An elementary oscillator is shown in the scheme 6.

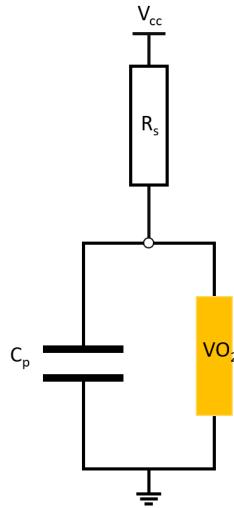


Figure 6: Electrical model of  $VO_2$  based oscillators

The oscillators are basically a phase changing device made of  $VO_2$  in parallel with a capacitance, all of this in series with a resistor. At first the material is in insulating state. When a DC voltage is applied to this system it is considered that the current going through the  $VO_2$  switch will produce enough heat through joule heating that it will cause the phase change, once it reaches the transition temperature. The phase change is accompanied by a drop of voltage along the switch, so a drop of joule heating, which will let the switching element to cool down. Once it is below the critical transition temperature the material

goes back to the insulating state restarting the cycle. The value of the series resistance (noted  $R_s$  in figure 6) is important since it will bias the system to the oscillating point. More precisely the value of the series resistance has to be chosen so that the load curve defines an operating point in the differential negative resistance part of the IV curve of the switching device, as shown in the figure 7.

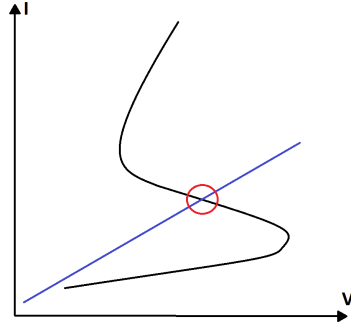
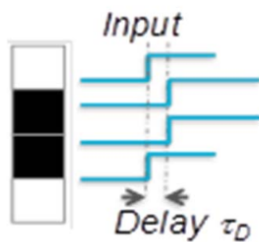


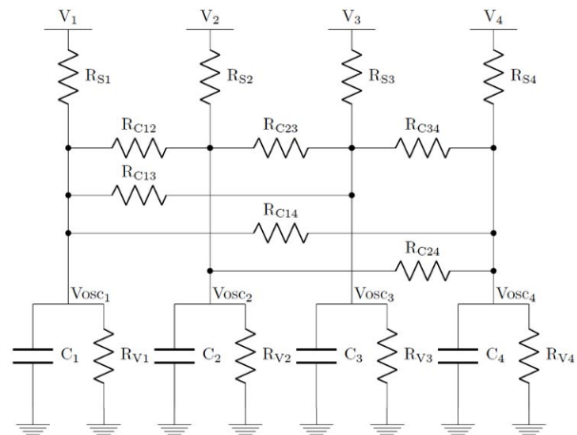
Figure 7: Typical IV curve example of a phase switching device (in black) with operating point (red circle), with load line from series resistance (in blue).

## 2.5 Oscillatory Neural Networks

To make a neural network out of the previously mentioned oscillators one can couple many of this oscillating systems with passive elements. Resistive or memristive coupling has the advantage of high area density and tunability. This resistive elements act as the weights of the network. Oscillators that are coupled together tend to lock in frequency. The difference of their phase is determined by the weights of the network i.e. the value of the coupling resistance. This is what enables the encoding of the information in the frequency domain for these systems. For illustration, an example of a oscillatory neural network that uses this principle is the one below.



(a) Pattern to memorize and frequency illustration.



(b) Example of network for pattern recognition.

Figure 8: Illustration of network and pattern recognition that can be done with this oscillating systems.[19]

By choosing the right coupling resistances, noted in the scheme 8b as  $R_{C_{ij}}$ , this network can be programmed to memorize a simple pattern as the one shown in 8a for example. With a further more complex 3 by 3 matrix of this "pixels" one can make a network that can recognize the  $a, b, c$  memorized patterns from the testing pattern  $d$  in figure 9.

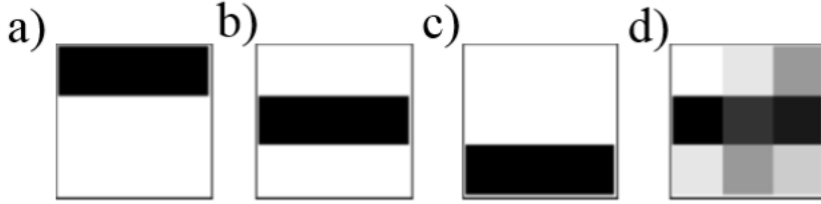


Figure 9: 3-by-3 patterns that can be used to memorize and train a network.[19]

The main challenge in the physical implementation of this network, is that the frequency-locking and the recognition performance are highly hindered by the device-to-device variability. Therefore, optimizing the fabrication process of the  $VO_2$  material and devices is essential to further develop this technology.

### 3 Motivation and Objectives

The motivation of this thesis as anticipated in previous chapters, is to fabricate reliable  $VO_2$ -based oscillators with the aim of designing Oscillatory Neural Networks for image recognition applications.

For this we have to develop an in-house fabrication process of  $VO_2$  films and try to reduce the variability among different  $VO_2$  based oscillators coming from the same film by engineering the process. This is a prerequisite to form reliable and predictable oscillating neural networks (ONN). Ideally, applying the same voltage to identical oscillators should result in the same oscillating properties (frequency, threshold voltage, etc...) but the granularity of  $VO_2$  films on Si leads to a device-to-device variability which makes the fabrication of ONNs difficult. This led to the main objectives of this work:

1. Investigate the  $VO_2$  deposition process and annealing conditions on  $SiO_2/Si$  wafers to gain control over the film morphology.
2. Develop and improve device fabrication from the improved  $VO_2$  films. In particular, exploration of different device architectures to find which is best suited for our purpose.
3. Gain an understanding of the mechanics of conduction of this material when deposited on silicon.

In the scope of this thesis, I developed an in-house deposition process of  $VO_2$  on  $SiO_2/Si$ . I have investigated the flash lamp anneal techniques for the crystallization of our films. Each film was measured with Raman spectroscopy to determine the vanadium oxide composition, and with Atomic Force Microscopy (AFM) and a Scanning Electron Microscope (SEM) to characterize the surface morphology. Finally the resistivity of the films has been characterized with a 4-probe measurement technique.

Afterwards devices have been patterned and etched from our best films, in two different architectures, a planar architecture and a three dimensional architecture, both introduced in the previous section. The point in this part is to see which architecture is best suited for the fabrication of oscillators characterizing them through current sweeps and temperature sweeps. The best performing devices are used to make oscillators

For the theoretical part we propose both a model and a toy model simulation to try to understand the complex nature and the different parameters that come in play when fabricating these devices in such a framework.

## 4 $VO_2$ Thin films

In this section we will describe the process of fabrication used to make the thin films. We will explain the materials used and the results that we got in the ALD, we will also reveal the design space that had to be explored for the flash lamp anneal step. In a first part we will introduce the processing and the tools used, we will explain our process and our protocols for the fabrication of this films and in a second part we will talk about the results we obtained.

### 4.1 Introduction

As mentioned before the processing is composed of an atom layer deposition of vanadium oxide followed by an anneal step to make crystalline vanadium dioxide. For the ALD step, we use tetrakis[ethylmethylamino]-vanadium (or TEMAV) as a precursor for vanadium and for the oxygen we explore three different precursors: oxygen plasma, ozone or water. Oxygen plasma and ozone were explored as a preferred solution, as these precursors do not contaminate the ALD chamber as much as water. After a water deposition, in fact, the chamber has to be pumped for two days to be available for other users again.

Then we do an anneal step to create the right compound of vanadium oxide, namely  $VO_2$ . The anneal process can be done either with a slow thermal anneal, which is the one option that can be found profusely in the current literature [16, 18, 31, 30]. But in our case, for research purposes, we will use a fast thermal anneal: the flash lamp anneal technique or flash anneal (FA). In fact, FA has demonstrated to be useful to stabilize other types of phase change materials [35]. The FA technique is a thermal treatment generally used for semiconductor processing. It is characterized by very strong temperature gradients along the thickness of the sample during the annealing process, mainly the surface of the sample is heated through a short but powerful flash, preventing the substrate to be heated too. This is advantageous for the annealing of thin films, it is also generally faster (the flash duration is around 1 ms) and consumes less power than normal heating. The working principle of the FA is rather simple. The whole sample is heated to a relatively high temperature with the help of an  $H_2$  lamp heater. Generally the sample is maintained in an inert atmosphere of  $N_2$  or in vacuum, for instance. If some active gases are needed one maintains the sample in a  $O_2$  filled atmosphere, which is our case. Then a capacitor/inductor system is charged and then discharged through a Xenon Flash lamp causing the annealing of the sample. The capacitor/inductor pair determines the time of the anneal. Then the whole system is cooled back down to room temperature. The scheme of a common FA tool can be seen in figure 10.

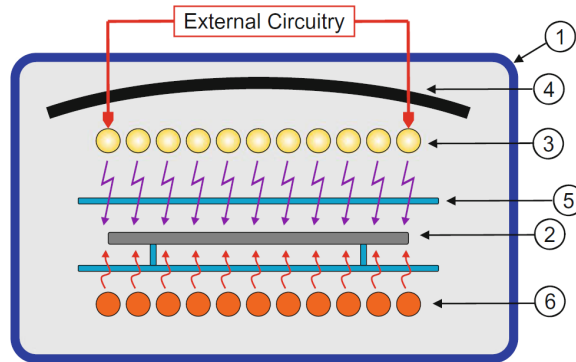


Figure 10: Scheme of a common FA tool. 1) Chamber, 2) Sample, 3) Flash lamp, 4) Reflectors, 5) Quartz window for protection, 6) Back side heating system.[34]

We are using the flash lamp annealing system FLA-50AS/150PH from Dresden Thin Film Technology.

As one can see in figure 11 our system is very similar to the one shown in the previous scheme. The system has a Xenon flash lamp (see figure 11d) on the upper stage that can be lifted up and down to open or close the chamber. Inside of the chamber there is a wafer holder for up to 6" wafers, and below it is the  $H_2$  lamp heater. Since we are mostly annealing small samples like 2cm\*2cm chips, we put a silicon substrate that serves as base, over it we put 3 chips of quartz which will serve as holders for the quartz disc that protects the whole lamp system from any pollution coming from the sample. Once the sample is sandwiched between the Si wafer and the quartz the chamber is closed and the anneal performed. Three parameters can be optimized for this process: the power of the flash, the temperature of the holder and the amount of oxygen we put inside the chamber. This is the design space that has to be explored to make

our own samples. To these three parameters we might add possible degrees of freedom like the time of the flash which can be adjusted by changing the capacitor and the inductor, but generally we maintained this fixed with 20 ms to limit our parameters. Another possibility is to do multiple consecutive flashes on the same sample.

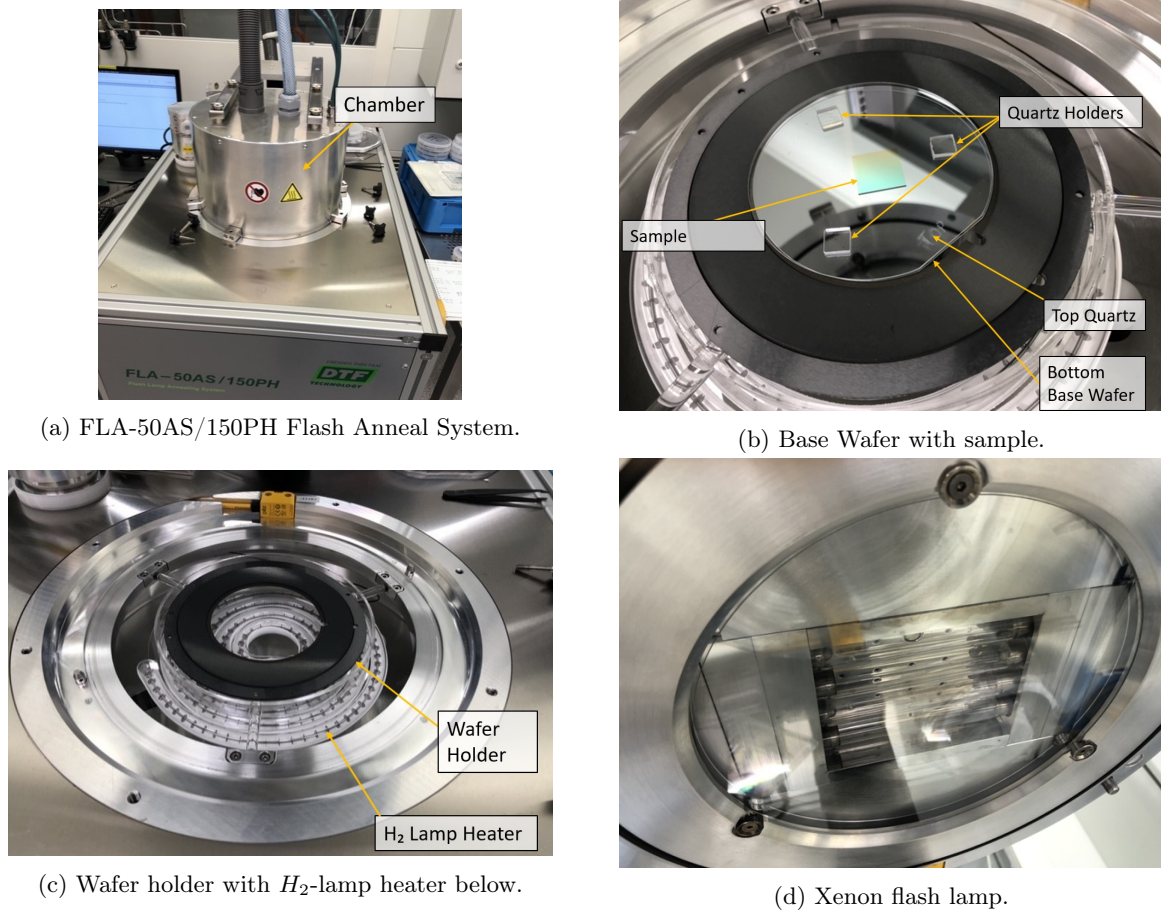


Figure 11: Flash Annealing System.

Our mode of operation was the following: first we would deposit some material in a 4-inch wafer which we would later cut out in many different pieces, mainly 2cm\*2cm squares. Some of this squares we would cut them using a diamond tip to make more smaller pieces. Trials in the FA would start with the smaller pieces to be able to make as much experiments as necessary. For each experiment we will use a Raman spectroscopic tool to see what compound had been created and to decide which conditions we would use in the following experiments. Once we obtained satisfying results we would move to trials with 2cm\*2cm chips, since these are the dimensions of the chips that we would later pattern to make devices.

For reference we put in figure 12 the Raman spectra belonging to different stoichiometry of vanadium oxide taken from literature [see figure 12]. We suggest the reader to reference back to this figure whenever we show our Raman results to understand our resulting Raman spectra.

After the material fabrication the topology of the film is studied under an AFM setup and a SEM when possible. The SEM was not always possible because sometimes the granularity of the film was not evident, the topology of the smoothest films was not resulting from SEM imaging. When all previous results were satisfying, we conducted resistivity measurements of the films.

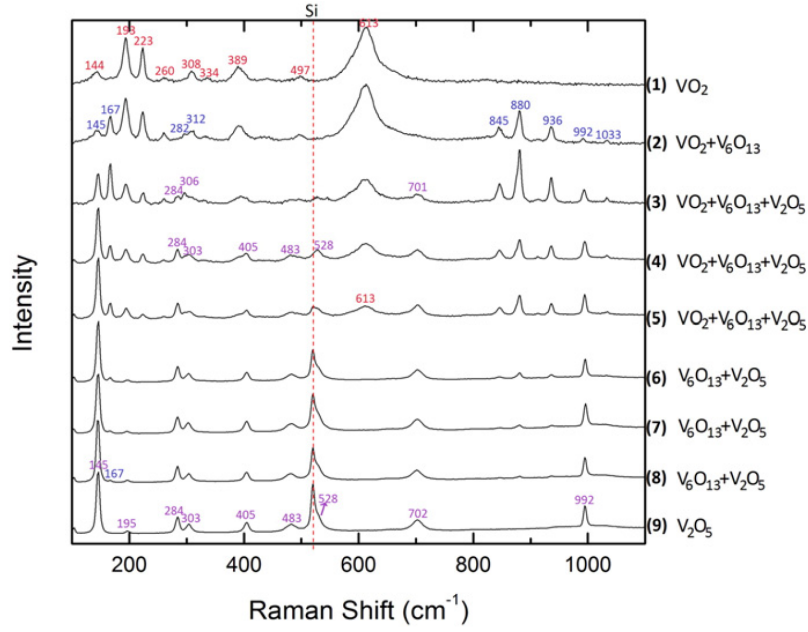


Figure 12: Raman shift for different stoichiometries of vanadium oxide.[33]

For the Raman spectra a NT-MDT NTEGRA Spectra device was used. For the AFM a Veeco Metrology System and for the SEM a Hitachi SU8000 system were used.

For the electrical characterization of the films a Meerstetter temperature control (TEC) system was paired with a Peltier element and a thermal sensor to be able to control temperature sweeps. This TEC system was in turn paired with an Agilent system for the recording of the electrical data. All of this was coordinated with a Labview program to make the measurements. The resistivity measurements were done by using a four probe measurement configuration of equally spaced probes as shown in figure 13. To be able to place the probes at an equal distance we used a "ruler" chip which consisted of a patterned chip where various "rulers" where patterned with equally spaced marks where we would place the probes. In such a configuration we apply a current through the outer probes and we measure a voltage in the inner probes.

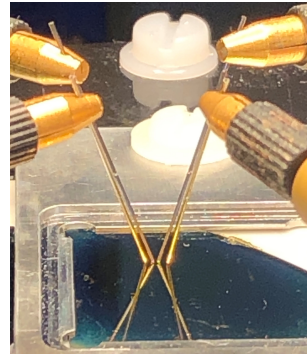
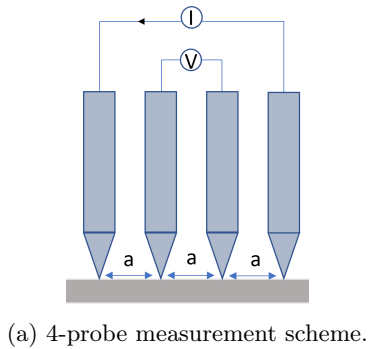


Figure 13: 4-probe measurement setup.

With this configuration we measure a resistance and we can easily calculate the corresponding sheet resistance as follows:

$$R_s(\Omega) = \frac{\pi}{\ln(2)} * \frac{V}{I} \quad (1)$$

Where  $R_s$  is the sheet resistance in  $\Omega/\square$ ,  $V$  the measured voltage in V and  $I$  the applied current in A.

And then we can compute the resistivity of the material through the following equation:

$$\rho = R_s * t \quad (2)$$

$\rho$  being the resistivity, generally in  $\Omega \cdot \text{cm}$ ,  $R_s$  the sheet resistance and  $t$  the thickness of the sample. In theory this method should eliminate the extra contact resistance that we would have if we would measure the voltage directly from the two probes that are used to apply the current, making this method more exact for resistivity measurements.

Below we offer two pictures showing the whole setup.

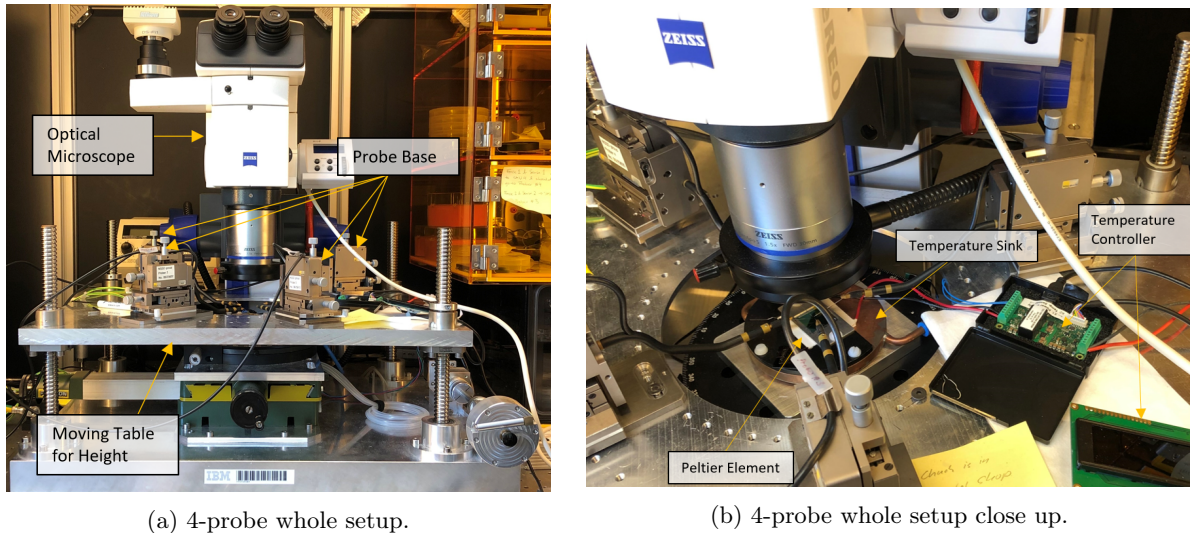


Figure 14: Resistivity setup.

Some features of the set-up impact on the precision of the conducted measurements. In particular, the measurement accuracy depends on the fact that the distance between the tips has to be the same. The usage of a "chip ruler" to align the probes to a certain distance has a limited precision, and therefore adds uncertainty to the measurements. A commercial probe set-up with fixed distance has been ordered in the frame of this project, to solve this issue, but it was not yet installed in the time-frame of this thesis. Uncertainty of this measurements will be further discussed in the next chapters.

## 4.2 Results

In this subsection we will explain the results of our processing experiments. First we will go over our preliminary and initial results with oxygen plasma and ozone based processes which mainly gave negative results. Then we will explain our more positive results with the water based process with two different thicknesses of deposited films: 26nm and 46nm of amorphous vanadium oxide. Finally we will explain our collaboration with EPFL's Nanolab where we explored the FA for germanium doped PLD deposited samples.

### 4.2.1 Ozone and Oxygen Plasma based process

First the oxygen plasma was tried out as a source of oxygen. This one was quickly abandoned after it produced directly  $V_2O_5$  before the anneal step. Subsequently deposition with ozone was tried. The deposition was done with different ozone times and for different film thicknesses. Then the flash anneal was done with conditions that were calibrated in a previous collaboration with University of Cambridge (UCAM). The results are to be found in figure 15. The most relevant results are to be found in the 10s of ozone time, this was applied to different thicknesses of  $VO_x$  and it was found to be effective and reproducible for low thicknesses, but not for higher thicknesses.

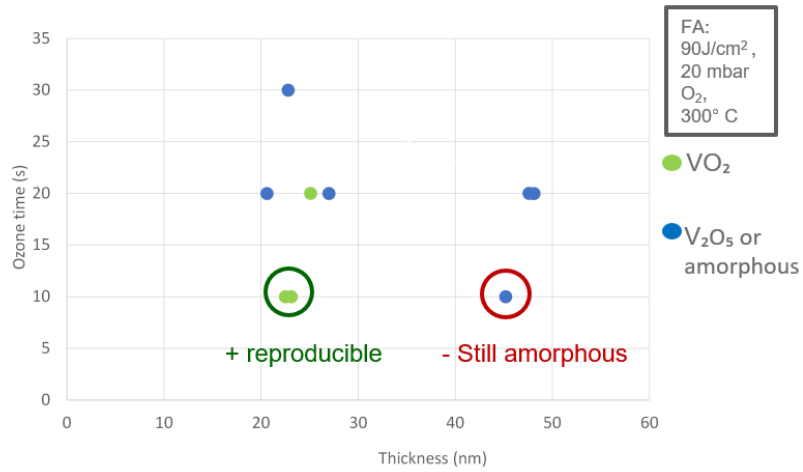


Figure 15: Results of flash anneal done with different ozone conditions for the ALD.

Given the promising preliminary results for very thin films, the flash anneal design space for the ozone-deposited samples was further explored on the 50nm thick film. The results are shown in figure 16.

As mentioned before, the design space, features mainly three variables: pressure of oxygen, power of the flash and temperature. From now on we are going to address the FA conditions with the triplet **FA(Pw,T,Pr)** where the Pw is the power of the flash in  $J/cm^2$ , the T is the temperature in Celsius and Pr is the  $O_2$  pressure in mbar. For example for an anneal done with  $90J/cm^2$ , at  $300^\circ C$ , with 20 mbar this conditions will be addressed as FA(90,300,20) with the previous notation. If nothing else is added this means that only one flash was done with the concerned chip and that the flash duration was of 20 ms. The size of the sample being annealed is also important and it will be pointed out before every experiment.

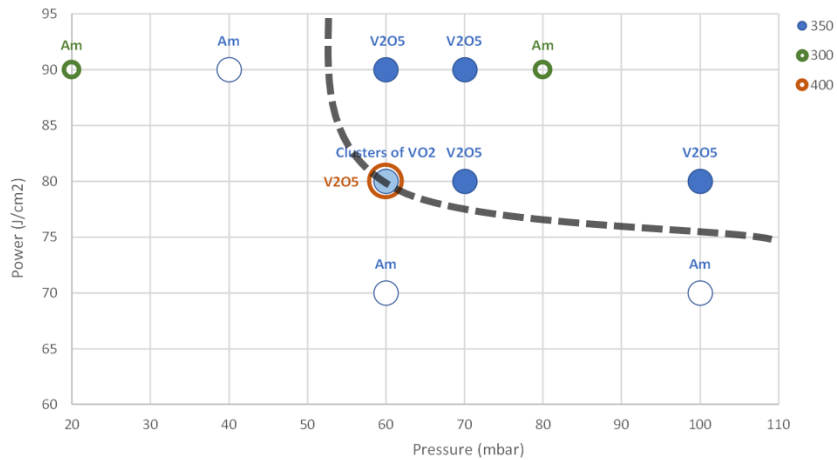


Figure 16: Results of different flash anneal experiments done on ozone samples.

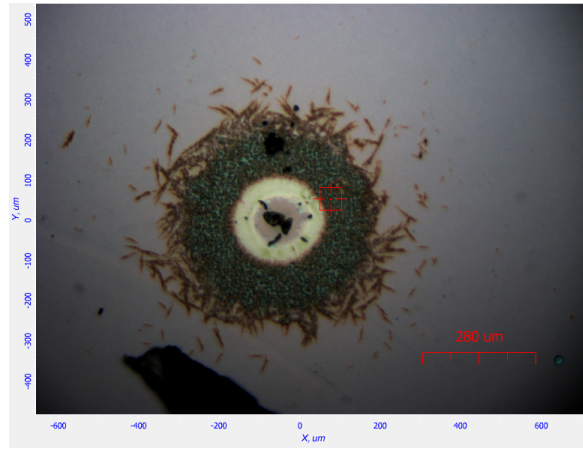
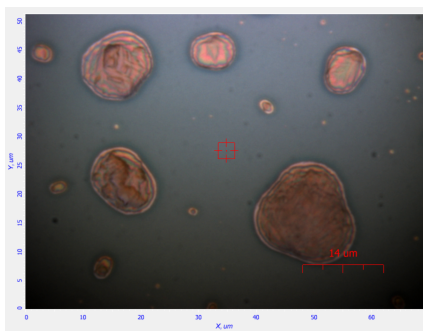
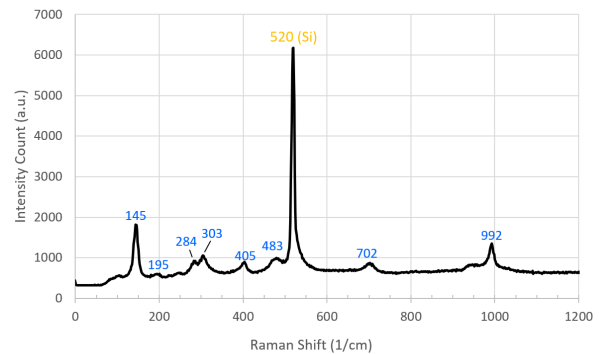


Figure 17:  $VO_2$  cluster.

Initially the annealing conditions tried were the same that proved successful for our partners, namely  $90J/cm^2$  for the power,  $300^\circ C$  for the temperature and  $30mbar$  for the oxygen pressure. At the beginning the temperature was not enough to anneal the films, this is represented by the two green circles. This two green circles show that within a wide range of pressure in the  $300^\circ C$  plane there is no anneal. The power we were using to anneal ( $90J/cm^2$ ) was already over the recommended maximum power that caused wafers to break in our system, so essentially we could not go to higher power. Therefore higher temperatures were tried. We started doing trials in the  $350^\circ C$  plane. With different power values and different oxygen pressure. It is important to point out that the dotted line represent two zones in this  $350^\circ C$ -plane where the material is either not annealed or becomes  $V_2O_5$ . In the line that separates these two outcomes there is one annealing set of conditions that resulted in a strange formation of highly concentrated  $VO_2$ . For these conditions we found that  $VO_2$  was indeed formed, but in the form of clusters, which are shown in figure 17, outside of this clusters the material stayed amorphous. These formations are not good enough for the fabrication of devices, since they form in an apparent random fashion and would make the patterning of many devices in the same chip difficult or even impossible. To finally discard the ozone based process combined with the FA we tried the same conditions of power and pressure but in the  $400^\circ C$  plane. This resulted in the formation of  $V_2O_5$ . An example of what was obtained during this experiments is given in figure 18a.



(a) Bubbles formed of  $V_2O_5$  with ozone based process.



(b) Raman spectra of the  $V_2O_5$  bubbles.

Figure 18: Example of  $V_2O_5$  produced with the ozone based process, and the Raman spectra obtained.

Then to see if the problem actually was the annealing technique we did some experiments with the classical "slow" anneal, results are shown in the figure below.

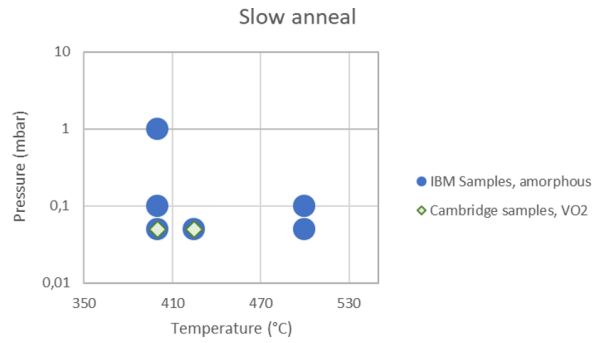


Figure 19: Slow Anneal Results.

For this slow anneal we tried different conditions, some that were known to have worked for our partners in Cambridge University (green squares in figure 19), but none gave the results that we wanted. As a conclusion, the ozone-based process proved to be unreliable and was thus abandoned in favour of the water based process.

#### 4.2.2 Water based process

For the water processing we proceeded with two different thicknesses of  $VO_x$ , 26nm and 46nm. For both of these thicknesses the results were positive after anneal,  $VO_2$  was produced as was shown by their Raman Spectra.

##### a) 26nm Thick Films

First we started with small chips of about 1cm\*0.5cm with 26nm of deposited material, the results with these small chips were positive. The triplet (90,300,20) gave a seemingly smooth and continuous surface of  $VO_2$  so we moved on with trials with 2cm\*2cm chips starting with this FA conditions. Results on the 2cm\*2cm experiments are shown in the figure below:

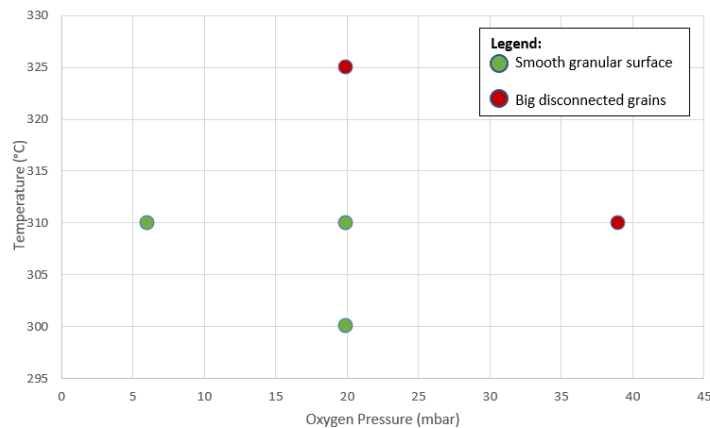


Figure 20: Flash Anneal results with 26 nm thick vanadium oxide with  $90 \text{ J/cm}^2$ .

The results on the bigger chips were as positive as the ones with the smaller chips as was shown by the Raman. There were two kinds of results: on the one side we produced seemingly smooth films, highly reflective to the naked eye yet still  $VO_2$ , then in the other side there is this very granular films.

In the case of the smooth morphology to get a better idea of the roughness of the sample an AFM scan was done.

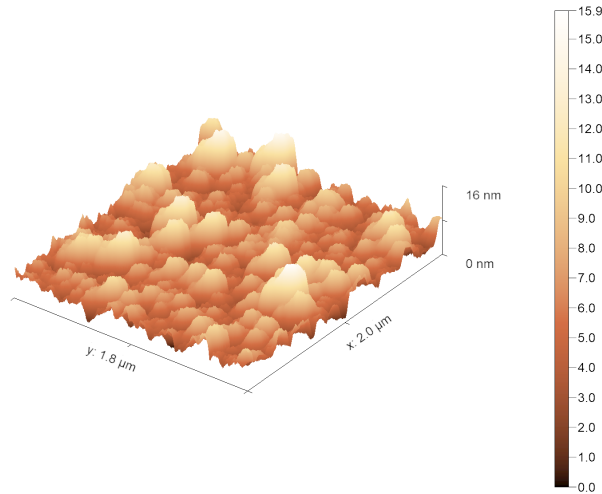
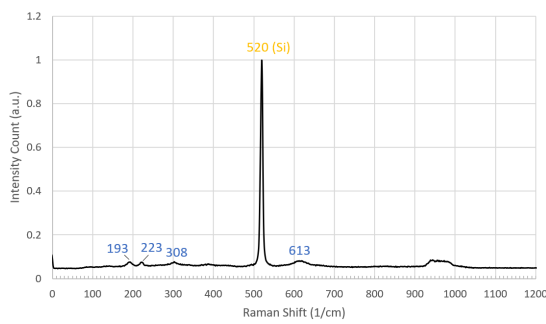


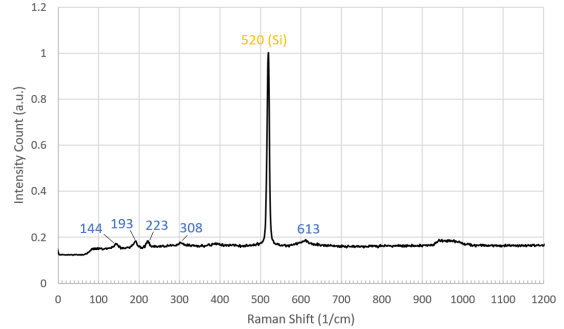
Figure 21: AFM of FA(90,310,20).

As shown in the figure 21 one can see the granular topology of the material and how relatively smooth the sample is with heights up to 16nm.

In both cases the resulting material was  $VO_2$  and their Raman showed slightly different spectra.



(a) Raman spectra of FA(90,300,20) with 26 nm of water deposited  $VO_x$ .



(b) Raman spectra of FA(90,325,20) with 26 nm of water deposited  $VO_x$ .

Figure 22: Example of Raman spectra obtained with two different condition triplets, (a) is a triplet that gave smooth surface (b) is a triplet that gave big grains.

The two different spectra give some preliminary information about the material quality we produced with such conditions. Given the peaks it is easy to point out that the compound in question is indeed  $VO_2$ . The first things that pops to the eye is the relative height of the  $VO_2$  peaks, big grains show relatively higher peaks vis-a-vis the Silicon peak in the Raman spectra. Furthermore there is an extra visible peak in the right side spectra, the  $144\text{ cm}^{-1}$  peak. This might signify that the quality of the crystal gets better with higher annealing temperatures which comes in agreement with what is found in literature [36]. Also there is a small chance that some  $V_2O_5$  has also been produced since it has a very strong peak at about  $145\text{ cm}^{-1}$  which is also a possibility which has been found in literature. One last thing that can be said about the big grains is that the Raman spectra is slightly more "noisy" than the smoother one which in the case of  $VO_2$  it has been found to unveil the presence of higher quantities of oxygen [37] in the material which could be pushing the creation of  $V_2O_5$ .

We have to point out the fact that only the smooth films are useful for the fabrication of devices since they consist of continuous material, and only then a patterning of devices is possible. In the more granular ones the material is disconnected and therefore it is not possible to pattern something out of this, and the fabrication of device is only possible by contacting through a lithographic step. So we could only characterize the resistivity of the smooth films with our setup.

In the end the electrical characterization of the best, smooth films was done as we show in figure 23.

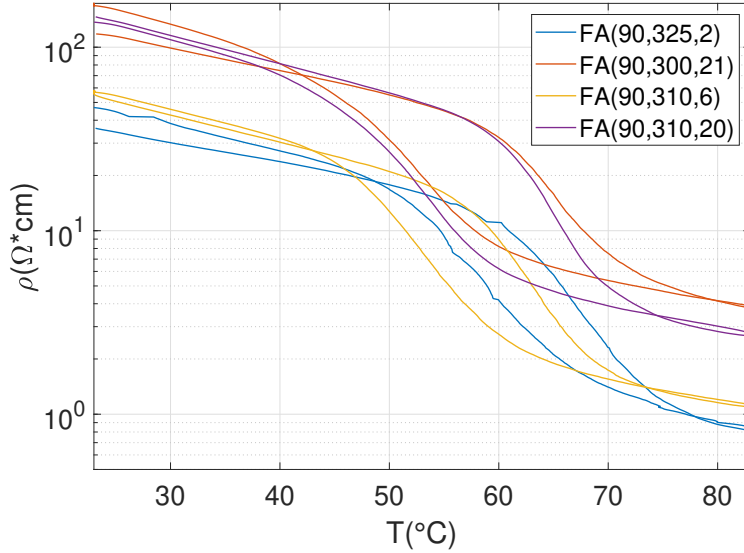


Figure 23: Resistivity measurement of 26nm deposited material for different conditions of FA.

The values of resistivity for these films are two orders of magnitude higher with what one can find in the literature for films on Sapphire substrate [13] or just one order of magnitude higher compared with  $VO_2$  on Silicon with buffering layer [38] and with a very small jump of resistance of about one order of magnitude. Nevertheless a phase change can be seen around  $60^\circ C$  which shows that the films consist indeed of  $VO_2$ . Probably the high resistivity and the small difference of resistivity between metallic and insulating state of the film might be caused by a poor crystal quality of the material.

Another point that has to be mentioned is the fact that we don't have a way to know the thickness of the material that was annealed, i.e. the portion of the material that conducts. Since the flash anneal has this characteristic that it anneals almost exclusively the surface of the material due to its high gradients of temperature one could argue that one of the reasons that the Raman is so poor for these materials is that only a few tens of nanometers of the material were annealed. Which would also explain why these films are so smooth.

The thickness of the conducting film is important because of equation 2, if the thickness of the film that participates in the conduction is lower than the thickness of the deposited material this would mean that we would have overestimated our resistivity values explaining why they are so high. This is another point that adds uncertainty to this measurements.

Additionally, some time after the annealing an aging of the samples was noticed, this was even more obvious in the samples with higher granularity, namely the ones annealed with the conditions FA(90,325,20) and FA(90,310,39), this was even more visible in the former due to a change of color than can be seen in the images below:



(a) Sample a few days after the FA.



(b) Sample after one week.

Figure 24: Aging effect of the 26 nm, FA(90,325,20) sample.

Having noticed this a second Raman spectra was recorded for both cases:

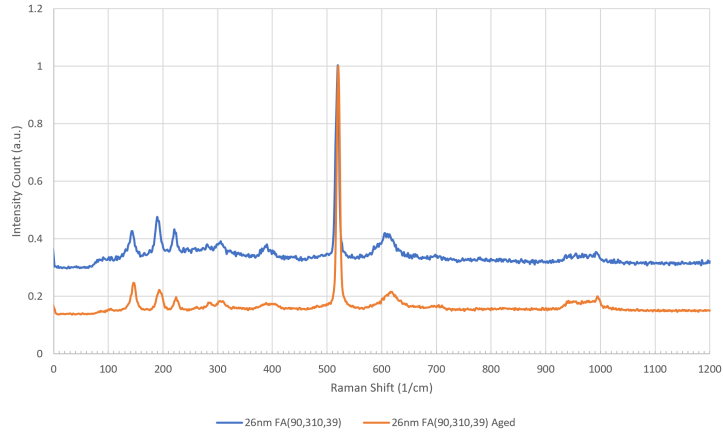


Figure 25: Raman of 26nm FA(90,310,39) before (blue) and after (orange) aging.

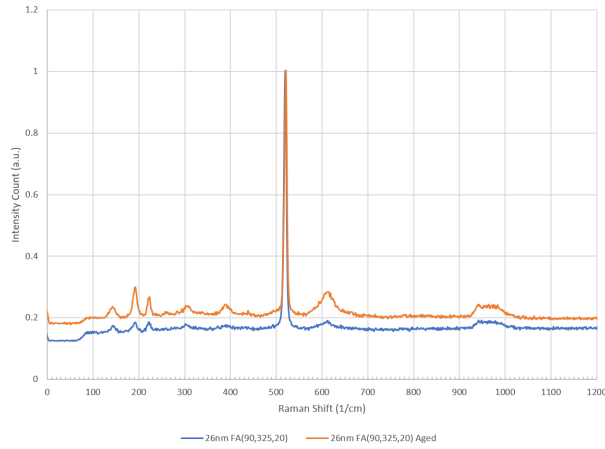


Figure 26: Raman of 26nm FA(90,325,20) before (blue) and after (orange) aging.

First for the high  $O_2$  pressure condition, namely FA(90,310,39) (see figure 25), we can see that after some time the peak around  $140\text{ cm}^{-1}$  grew. We say around  $140$  because it could be either the peak at  $144\text{ cm}^{-1}$  corresponding to  $VO_2$  or the peak at  $145\text{ cm}^{-1}$  corresponding to  $V_2O_5$ . It can be hypothesised that given the relative size of this peak vis-a-vis to the  $193$  and  $223$  peak, being bigger, it could be that the material is further oxidizing into  $V_2O_5$ . To this is added the peak at  $992\text{ cm}^{-1}$  that has become more visible in the aged sample, which supports the formation of  $V_2O_5$  theory.

For the other sample the FA(90,325,20) however the material has proved to be much more stable even with the change of colour shown in 24. In this case most of the peaks from the  $VO_2$  compound are more visible, specially the peak at  $389\text{ cm}^{-1}$  and  $613\text{ cm}^{-1}$ . The reasons for this are not yet clear, maybe some of the material is transforming into  $VO_2$ , or the material was polycrystalline and now it has become monocrystalline.

## b) 46nm Thick Films

For the  $46\text{ nm}$  thickness we started with the small chips as well, the results for this chips are shown below:

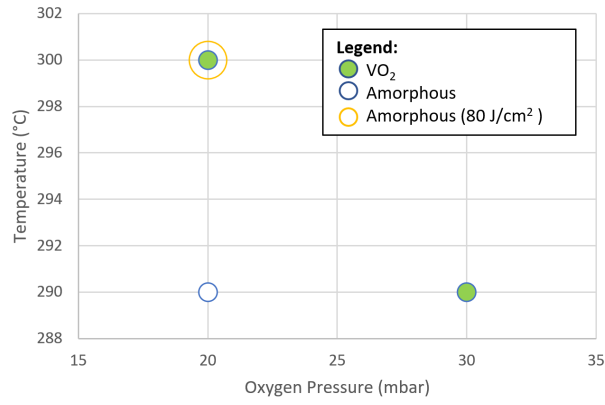


Figure 27: Flash Anneal results with 46nm, in small chips (if not pointed out the annealing was done with 90 J/cm<sup>2</sup>).

The results given by the triplets FA(90,290,30) were specially interesting for this thickness given that the middle of the chip gave the Raman peaks corresponding to VO<sub>2</sub> and the surface was very smooth as was shown by the AFM scan we did, shown in figure 28.

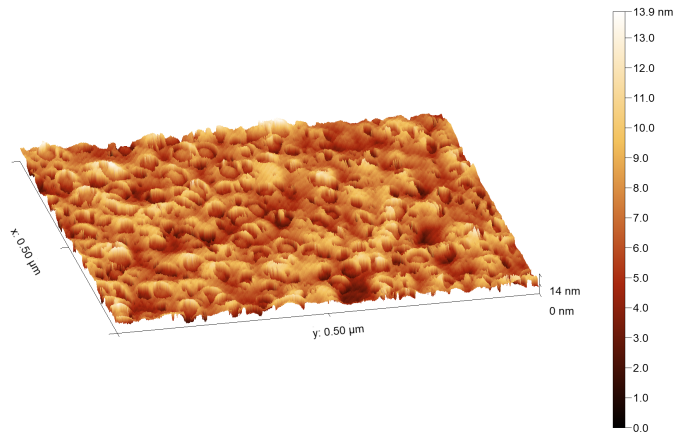


Figure 28: AFM scan of FA(90,290,30).

So we decided to proceed with the 2cm\*2cm. The results are shown in figure 29.

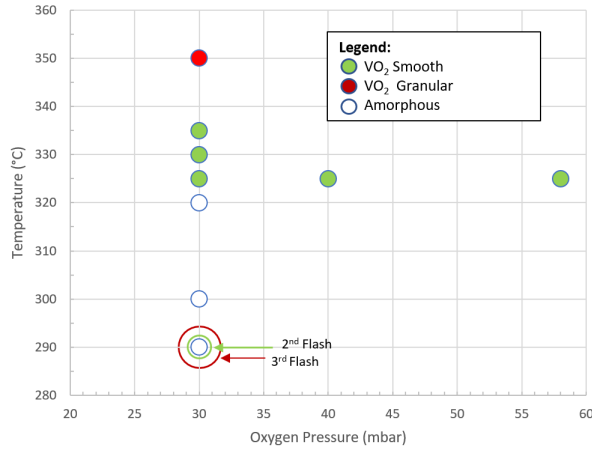


Figure 29: Flash Anneal results with 46 nm with  $2 \times 2 \text{ cm}^2$  chips.

For the big chips we started by trying out the previous triplet that gave good results. As after the first flash the material was still amorphous, we annealed it again at the same conditions. We were able at this point to achieve a seemingly smooth  $VO_2$  film. This showed that the dimensions of the chip could be an important parameter depending on the thickness of the deposited film.

Then we decided to do a third anneal with the same conditions, and this finally gave the big grain showing a certain pattern of evolution for any flash anneal conditions. Repeated experiments with two subsequent flashes gave different and not reproducible results. Therefore, it was decided for the subsequent experiments to abandon the study of multiple flashes and to optimize the 1-flash anneal process.

We proceeded with multiple experiments with the 46nm  $VO_2$  thick chips of  $2 \text{ cm} \times 2 \text{ cm}$ . Since the chips are bigger the annealing conditions had to be modified slightly, essentially we had to anneal at higher temperature. A temperature sweep was done with these chips to find the optimum temperature to fabricate the smoothest film with highest coverage of  $VO_2$ . Thanks to the contrast given by the different morphology this was not a difficult task. The results are displayed in figure 30.



Figure 30: Three different results of FA in the 46 nm thick films with results at  $90 \text{ J/cm}^2$  of power and 30mbar of oxygen pressure

As can be seen in the figure above the samples have very different zones with very distinctive colours. Essentially the blue/red part was mostly big grains, the light yellow part was amorphous material and the dark yellow part was our annealed smooth material. What was looked for was to get the most continuous dark yellow film. It was found that the most continuous film was obtained with  $327^\circ\text{C}$ . And would be interesting to try out for a whole  $2 \text{ cm} \times 2 \text{ cm}$  chip. This being said the effects of the FA not being perfectly understood, the results of our experiments can not be taken as a given. And could vary a lot depending on the conditions of deposition for example. We are merely showing what we observed, but this could change if we did the same experiments again, but due to constraints in time this was not possible. In any case, centering ourselves in the  $325^\circ\text{C}$  case we did the AFM of the dark yellow section, and we found a very smooth film with a more granular topology than the one observed in the FA(90,290,30) with the small chips shown in figure 28.

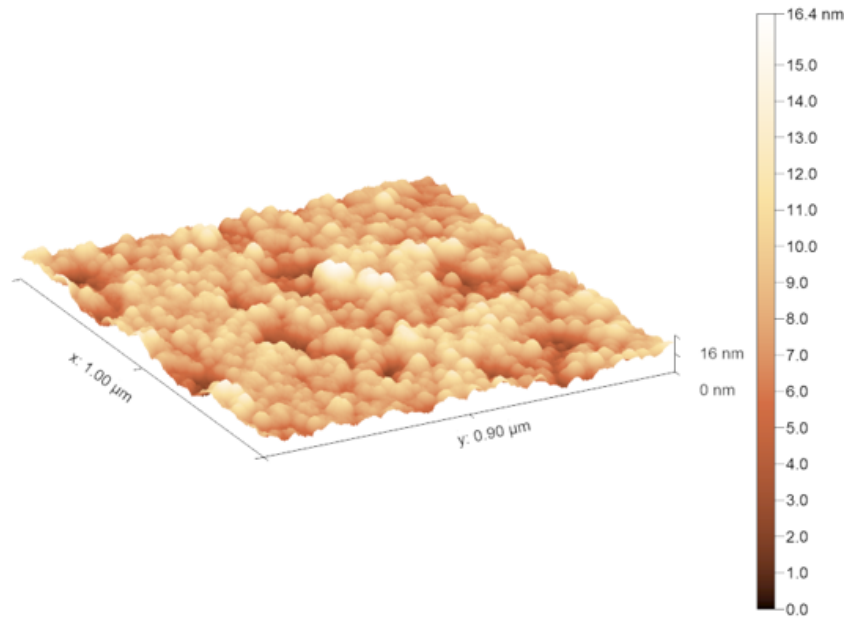


Figure 31: AFM scan of FA(90,325,30) showing a smooth film.

And the resistivity curve showed that indeed we had fabricated  $VO_2$ . With a phase change near the  $60^\circ\text{C}$ .

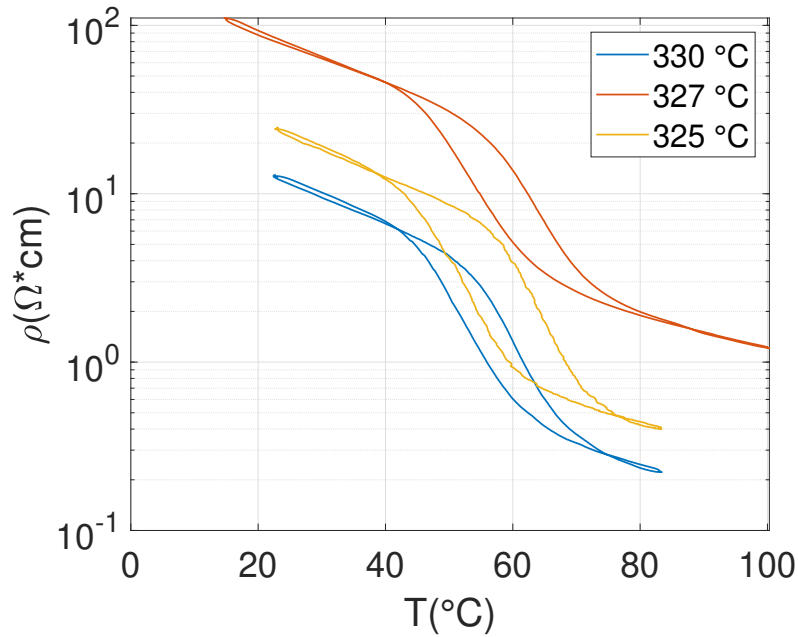


Figure 32: Resistivity measurements of ALD 46nm FA(90,325,30)

The same remarks made on the resistivity measurement for the 26nm thin films can be made here, the resistivity is one up to two orders of magnitude higher than the one that can be found in literature for films fabricated in Sapphire substrate. The situation where we may have overestimated the thickness of the conducting material is still the same, explaining why these values are so high. Why the films start a phase transition at around  $55^\circ\text{C}$  is a question we could not answer, but this might be because of some internal stresses in the annealed material.

### 4.2.3 Ge doped $VO_2$

As a last step in the material process exploration we undertook the task to explore the flash annealing of some germanium doped  $VO_2$  deposited through a PLD technique. The deposited samples were produced by EPFL's Nanolab as mentioned before. The material deposited was already vanadium dioxide as was showed in the Raman spectra of the sample (see figure 33).

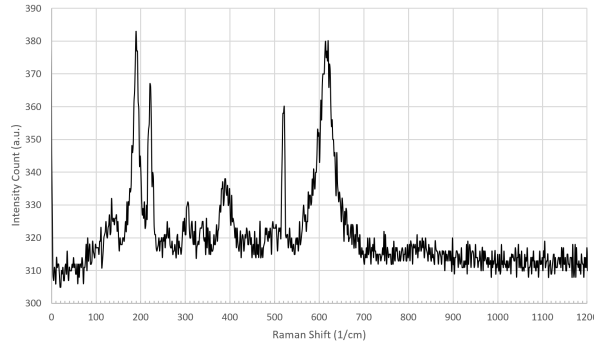


Figure 33: Raman of PLD deposited  $VO_2$  doped with germanium.

The FA experiments done for this samples are synthesized in the chart below.

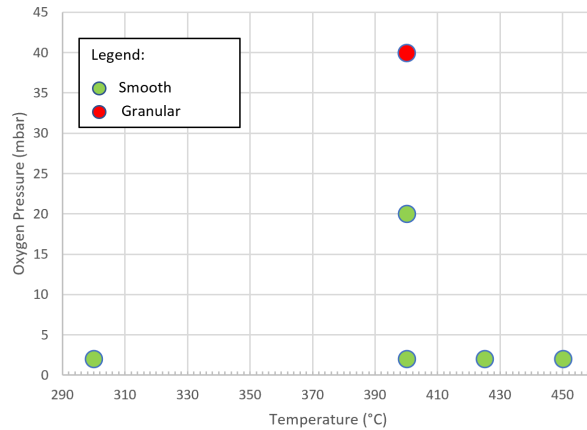
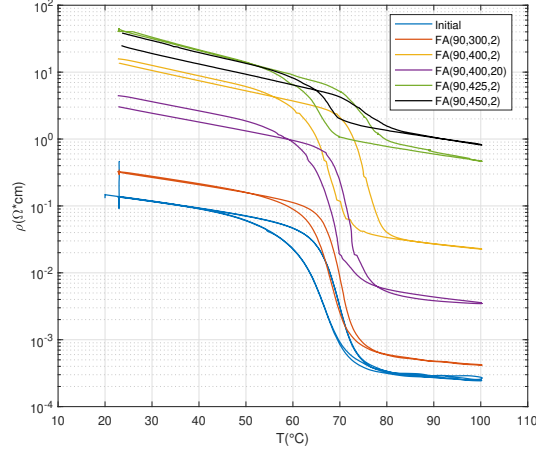


Figure 34: FA experiments done with germanium doped PLD deposited samples.

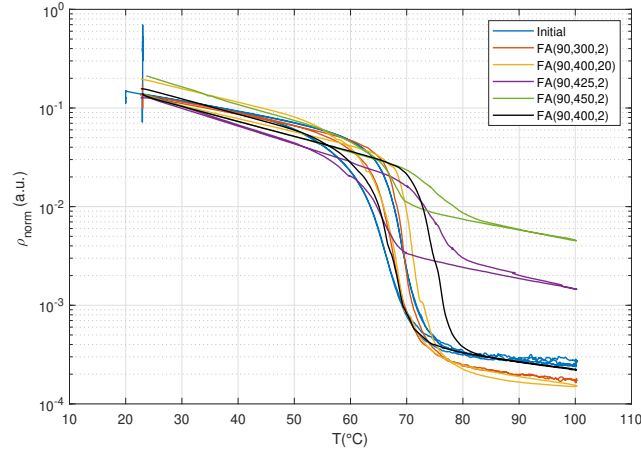
As it is shown the material is of very high quality the  $193\text{cm}^{-1}$  and  $223\text{cm}^{-1}$  peaks are very visible, also the Si peak at  $520\text{cm}^{-1}$  is barely visible.

With these chips many different conditions for the flash anneal were tried, since the material was already  $VO_2$  we were able to do a resistivity measurement of the initial sample, and moreover the Raman spectra was not of much interest since the material was kept in a  $VO_2$  phase so no real difference was observed in these measurements. Then the interest of this study was to see how much we could increase the MIT temperature for the films. As before the resistivity measurements could only be done in the smooth samples and a relevant difference was seen from the  $400^\circ\text{C}$  annealing temperature.

In the end we were able to obtain a maximum increase of  $10^\circ\text{C}$  for the IMT maintaining the same resistivity jump by annealing at  $400^\circ\text{C}$ , with  $90\text{J}/\text{cm}^2$  and 2mbar of oxygen pressure, higher temperatures where tested but this decreased the jump measured, and conserved the same IMT temperature. Flash annealing the samples at higher oxygen pressure only caused the material to become granular, and no resistivity measurement was possible. All of this is illustrated with the figures below where we show the absolute measured resistivities in figure 35a, and the normalized resistivity measurements with the initial resistivity for comparison in figure 35b.



(a) Resistivity measurements obtained with FA of Ge-doped samples.



(b) Resistivity measurements normalized for comparison with initial sample.

Figure 35: Resistivity Measurements for all the Ge doped samples.

### 4.3 Conclusion

In this chapter the ALD deposition of vanadium oxide films was explored utilizing three different oxygen precursors, plasma, ozone and water. It has been found that oxygen plasma led to deposition of  $V_2O_5$ , while the ozone process, despite some preliminary promising results, resulted to be hardly controllable when going to film thicknesses of around 50 nm. The water-based process was found to yield good and reliable results. We explored a flash lamp annealing technique to crystallize the amorphous  $VO_x$  film in the  $VO_2$  stoichiometry.

Many parameters have been considered during the process optimization. It was shown that we can control the material transformation from amorphous vanadium oxide to a smooth vanadium dioxide phase, then through a higher quality but granular vanadium dioxide phase, transforming finally to a vanadium pentoxide under high pressure or high temperature annealing conditions. The experiments were also conducted in Ge-doped films to engineer the transition temperature of the material.

The quality of the smooth films was not the best due to the tendency of the material to become granular. Probably this tendency makes the resistivity higher and could have an important impact on the patterning of devices later on. For further resistivity measurements set up improvements are in progress.

In the following we discuss and explore the possible devices that could be made out this films.

## 5 $VO_2$ Devices

It is important to be reminded that the purpose of the previously explained exploration of the fabrication of  $VO_2$  thin films is done to fabricate devices that could be used as oscillators.

In this section we will discuss more in depth the different devices that can be fabricated from this films. We will explore mainly two device architectures the planar one and the crossbar one. A third architecture, the singular grain, will be also explored as last possibility.

In a first part we will introduce shortly the processing that was undertaken for the fabrication of the devices. The setup made for this measurements will be also introduced. Then we will follow up with the results obtained for each configuration and we will explain how and why these designs may or may not be used for the fabrication of oscillators in the future.

### 5.1 Introduction

After the fabrication of  $VO_2$  we move on to the patterning of devices. For this we do two lithographic steps. The first one defines the dimension of a  $VO_2$  stripe, and it is followed by an ICP etching of the material. The second step provides the design for the contact of the  $VO_2$  device, achieved through evaporation of Ni/Au.

The device can be patterned in two configurations as mentioned before, a planar one where the device is a strip of  $VO_2$  with contacts on each side. Or a crossbar one, where the contacts are on top and below the film. An SEM image of the two kinds of devices are displayed in figure 36.

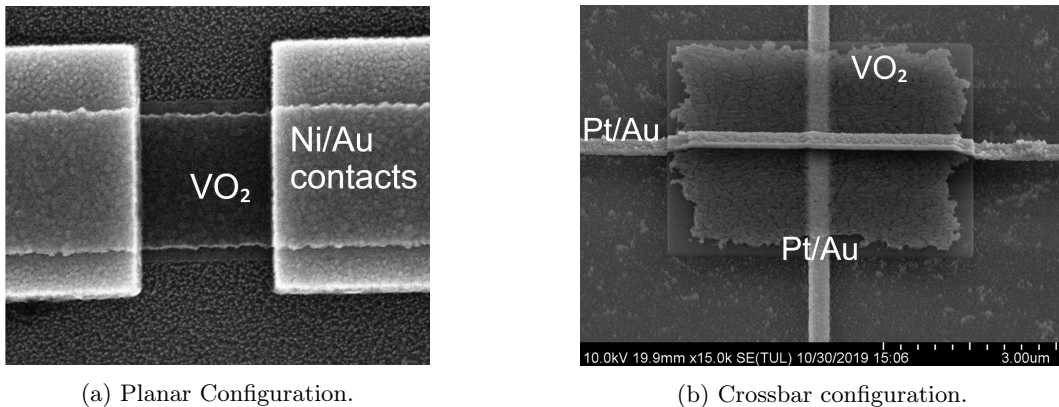
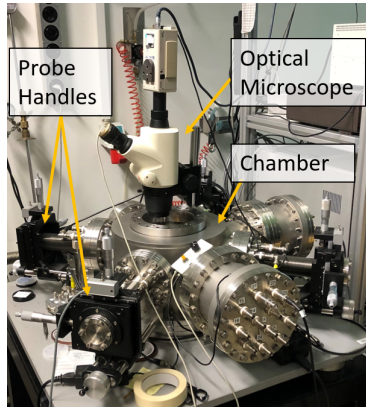
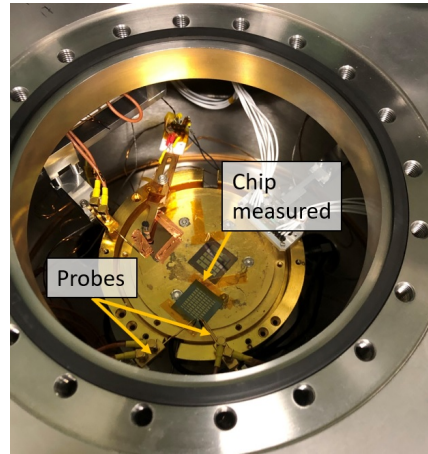


Figure 36: SEM images of two different patterned devices from  $VO_2$  thin films

For the characterization of this devices we did two kinds of sweeps: a sweep with temperature and a sweep with current. For this two sweeps the chip with the patterned devices was placed in a temperature-controlled chamber where it was immobilized using Kapton tape. The chamber had a temperature controller for the temperature sweeps, and one could easily contact the device with two probes as shown in figure 38. The whole setup and chamber for the characterization of devices is shown below.



(a) Vacuum Chamber used for characterization of devices.



(b) Close up inside the chamber.

Figure 37: Device characterization setup.

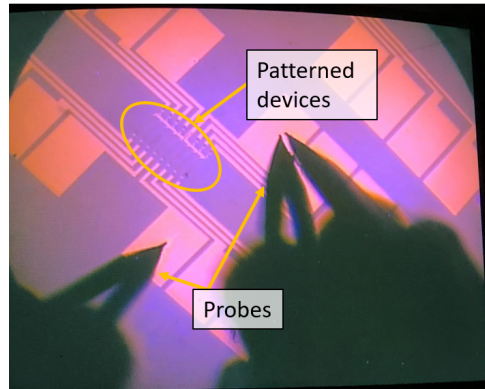


Figure 38: Optical microscope image for characterization of devices.

The characterization of the device is done to see if it could work as an oscillatory system. We do two characterizations, with temperature which shows a general behaviour of the device, where we expect to get a hysteresis and a phase change near  $64^{\circ}\text{C}$  and with current. Since the device will be, at least ideally, electrically activated, one has to characterize the behaviour of the device with a current source. If the devices behaviour was satisfying enough (i.e. showing a hysteretic behaviour in current and in temperature with a phase change at around  $340\text{K}$ ) the idea was to either use them to make oscillators by adding a capacitance and a resistor or sending them to be characterized by our colleagues who work on the thermal characterization using a novel Scanning Thermal microscope (S<sub>Th</sub>M) [39].

## 5.2 Results

### 5.2.1 Planar Design

First we tried the planar devices since this are the only ones that can be characterized through the S<sub>Th</sub>M setup. This where fabricated from UCAM deposited samples annealed in IBM six months prior to this thesis. Most of them didn't show any remarkable phase change. Most were either difficult to turn to a metallic state or the activation through current would generate so much joule heating at the moment of the transition without enough heat dissipation that the contacts would melt together or the material would break. Some of them did turn but the transition was so small it can hardly be counted as a transition and would be difficult to use them either for a thermal characterization or as oscillators. An example of this small phase changes is accounted in figure 39.

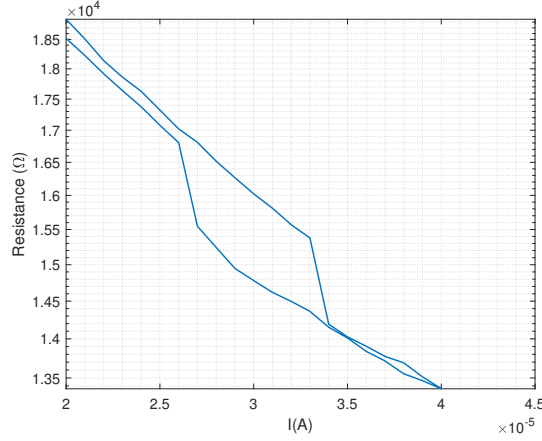


Figure 39: Planar device phase change.

It is considered that this jump in resistance is a phase change of the material because it is reversible, nevertheless the jump is too small to be considered useful for an oscillating device.

The low quality of our planar devices was first thought to be caused by the age of the devices since they were fabricated almost 6 months before to this thesis. It was thought that maybe the quality of the material had decayed or the vanadium dioxide had oxidized more than previously thought since it was kept in ambient atmosphere. In any case more than a hundred devices were patterned per chip and yet no device or almost no device showed a relevant phase changing effect.

Despite their poor reliability for the fabrication of oscillators we were able to submit these devices for their thermal study in the SThM which could be really useful for the understanding of the electrically activated phase change transition in the material.

Some planar devices were fabricated from the 26nm smooth films which we discussed in the previous section, namely from the FA(90,300,21) and the FA(90,310,6). None of these devices held significant performances, suggesting that said process is not enough for the fabrication of oscillators. Since there was a possibility that the annealed film, i.e. the conducting part of the film, was actually a small section of the whole film (which was in a way supported by the resistivity measurements) we believe that what happened is that the conducting layer was removed accidentally through the patterning process.

### 5.2.2 Crossbar Design

Subsequently we characterized some crossbar devices which yielded much better results in terms of current resilience and phase change. The devices were first subjected to a temperature sweep. After this some current sweeps would be made to get their IV characteristics. Since most of these devices showed an initial electro-forming cycle with an irreversible phase change and subsequently showed a permanent reversible phase change many current sweeps were done sequentially. An example of this is shown in figure 40. As we can see the hysteresis is below an order of magnitude but it is a clear hysteresis after the first cycle. This was one of the best examples of the irreversible phase change, the reason for this is not yet well understood but it could be that once a current is applied some granular domains tend to merge with each other due to joule heating making them more stable. A small study was done in these devices trying to compare the resistance vs temperature of the devices before and after the irreversible phase change. The temperature sweeps before and after the irreversible phase change are in figure 41.

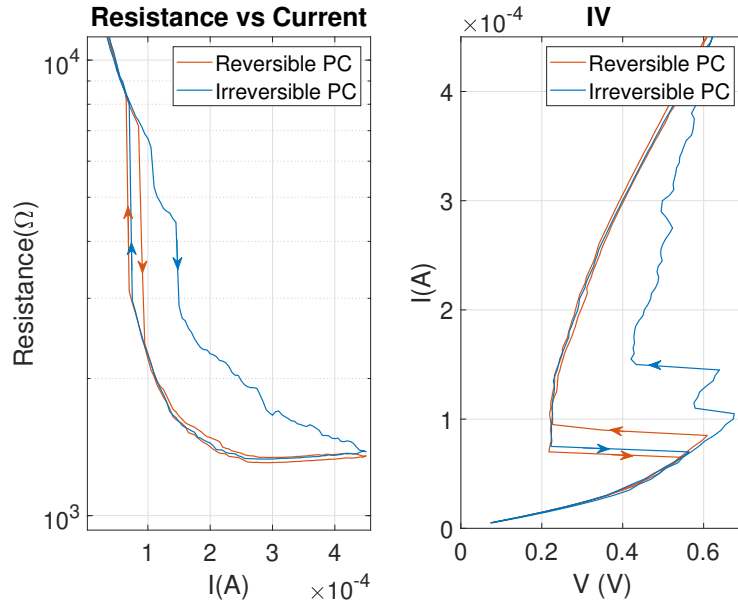
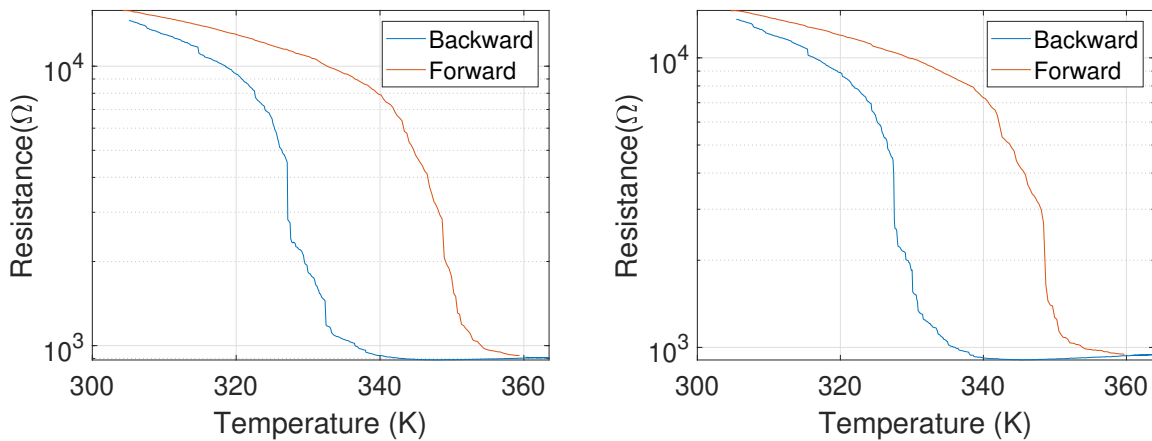


Figure 40: Resistance vs Current and IV curves through current sweep of device 2-10, we can see the irreversible phase change and the subsequent reversible state of the device.



(a) Temperature sweep before the irreversible phase change of device 2-10. (b) Temperature sweep after the irreversible phase change of device 2-10.

Figure 41: Temperature sweeps of device 2-10.

The idea behind this study was to have a better understanding on how these devices worked, since different devices in the same chip would have their IMT at different current values. We tried to look if there could be a clear relationship between their transition activated by current and their transition activated by temperature. One could try to isolate the resistance jumps for each grain using this information and try to link them through their resistance value, like this we may be able to identify which grains switch, and we would be able to link the equivalent internal temperature at a certain current value. This small quantitative study proved that it was hard to make a comparison between temperature activated and current activated change in resistance, which could be understood that both activation modes cause the MIT in radically different ways. A clear comparison is shown below on the device labeled 6-13:

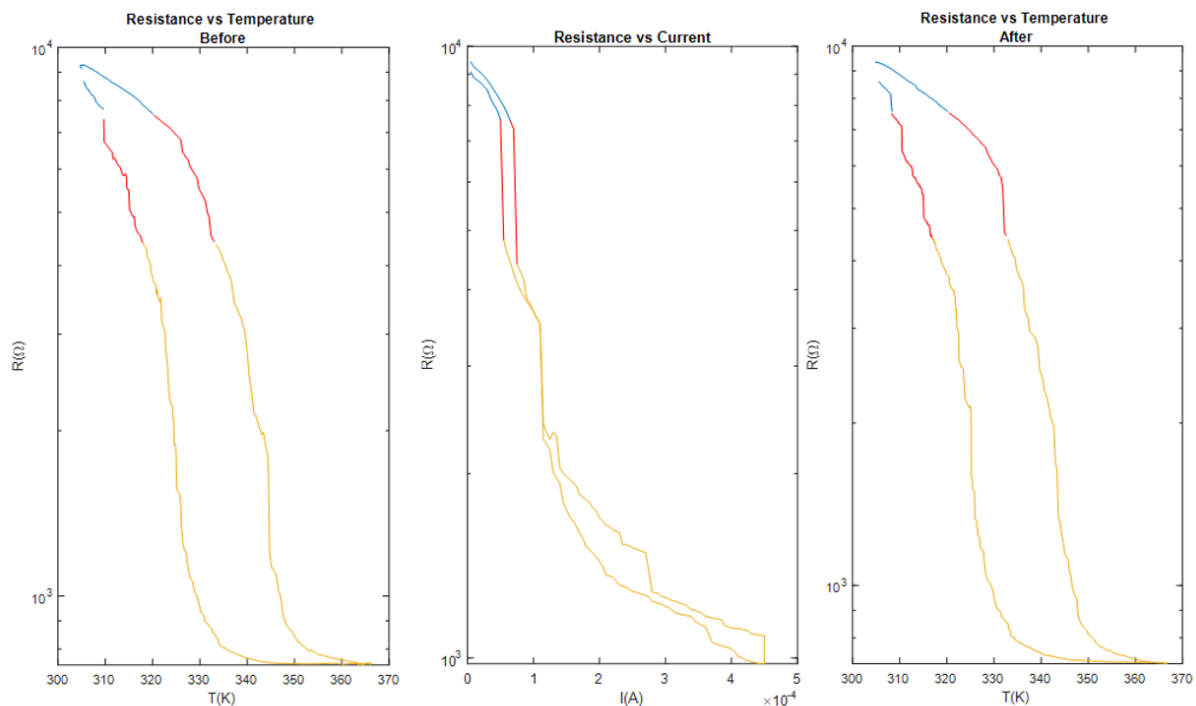


Figure 42: Quantitative comparison on the temperature activated and current activated phase change of device 6-13.

In the resistance vs current graph we show in red the first important resistance jump. We use this jump as reference. The idea behind this plot was to separate the "before" and "after" of the first important current activated phase change (colored in red), and to see if we could find a correlation in the resistance vs temperature sweeps before and after the irreversible phase change.

As one can easily see from figure 42 the difference between the two activation is obvious. First of all the jumps in resistance are bigger in the current activated switching, whereas the temperature activated is more gradual, there is a big amount of small steps. To make a precise correlation between these measurements, a statistical analysis over a large number of device should be made. While this is in the plan of the research project, this was ultimately not pursued between the scope of this thesis.

If we think about this devices as one grain thick layer sandwiched between two contacts, this is explained through simple thermal model that the devices were activated through Joule heating in the current sweep. The mechanics are thought to be as follows: for the current activation, at the beginning the grains inside of the device are all in a high resistance state where the current is dispersed through all the grains homogeneously, so the power dissipated by each grain is relatively the same. But when we arrive up to a certain current value a certain grain is forced to phase change. This might be because the grain was actually slightly less resistive than the others and so more current would flow through it, and so it would dissipate more heat reaching higher temperatures faster. Or it could be that this grain has the lowest phase change temperature. In any case it turns into a metallic state and the current will follow vigorously this preferential path and so the heating dissipated by this grain will be much more significant than the other grains that are still in the insulating state. This will have a sort of positive feedback loop effect heating the nearby grains turning them metallic and this ones will help turn their neighbours and so on and so fourth. In any case the point is that probably in both cases the heating is the cause of the phase change, but the difference is that the heating in the current activation is less homogeneous than in the case of the temperature sweep. In the case of the temperature activated switching the grains are all at the same temperature and they will simply turn when their phase change temperature is reached.

Anyhow, in theory one could extract from the resistance versus temperature plot the distribution of the phase changing temperature, but it is really difficult to try to define which grain is switching, making the variability of the devices difficult to control, since in the end one device consist of a whole system of many grains, it is a many body system that is rather hard to explain. A further discussion about this sort of toy model is done in the next section on simulation and models.

In any case using this configuration we were able to make many oscillators, showing an optimal

oscillating behavior. Then we used four of this oscillators and locked them in frequency, despite their strange waveforms, showing that this architecture has a lot of potential for the fabrication of oscillators. The lock in on the frequency is shown in figure 43 where we show first their waveforms and their Fourier transform below. In figure 43 the device were slow down by a capacitor to get good waveforms, but this devices can reach up to 2MHz in frequency which shows their big potential for this technology.

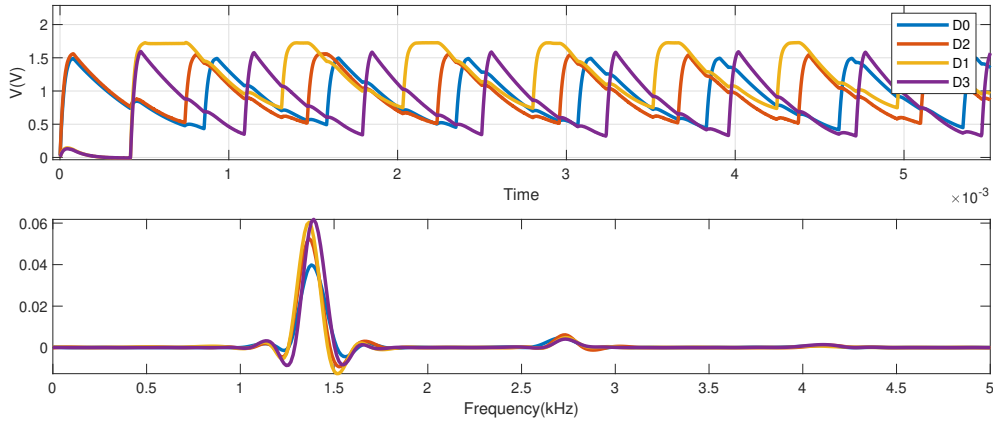


Figure 43: Lock in frequency of four crossbar oscillators.

Furthermore a last point that can be highlighted from this devices is that the smaller the contacts the more comparable they are to a single grain device (shown in the following subsection). In figure 44 we report two temperature sweeps from two different small crossbar device (of around  $125\text{nm} \times 125\text{nm}$  big).

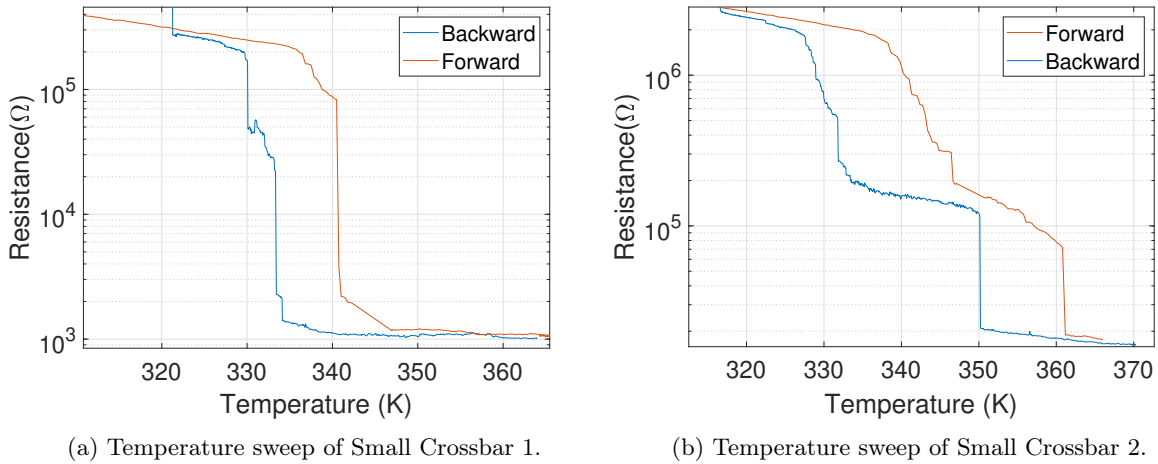


Figure 44: Temperature sweeps of two small crossbar devices.

This smaller version of the crossbar report a higher resistivity jump from two orders of magnitude at least and a relatively thin hysteresis of about  $10^\circ\text{C}$  of width. This shows a certain interest and utility of scaling down this devices.

### 5.2.3 Singular Grain

In a last experiment a couple of bubbles fabricated with ALD and the slow anneal procedure were contacted with Ni/Au contacts to see if these small, high quality crystals could be used for the fabrication of an oscillator.

During their initial temperature sweep these bubbles showed a remarkable steep hysteresis with a jump of almost 3 orders of magnitude in their resistance, much more important than the ones obtained with our films (sweeps shown below).

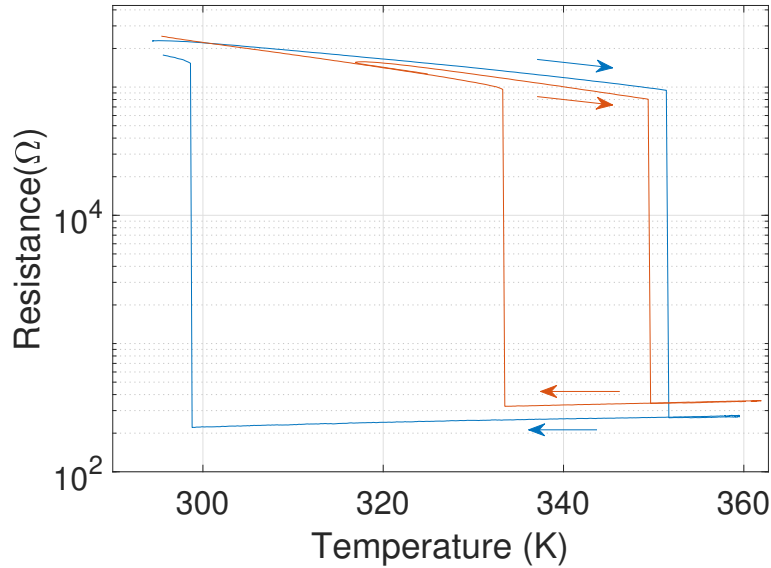


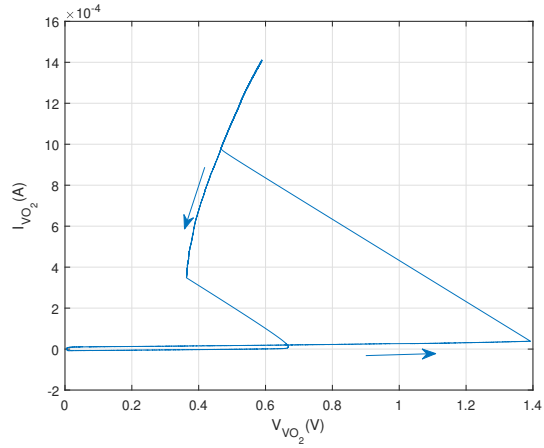
Figure 45: Resistance vs Temperature characteristics of two different bubbles.

One thing that is really important to remark is that the width of the hysteresis is very different between the two bubbles of the same chip. One of the bubbles had a hysteresis width of around 10 to 15 °C whereas another one had a width of more than 50 °C. The width of the hysteresis is an important factor because it will affect the maximum frequency one can reach with such a material and therefore affect the speed of computation of the oscillator. In short the smaller the width the easier it is for the material to go from one state to the other and therefore to oscillate. So it is an important phenomena to understand.

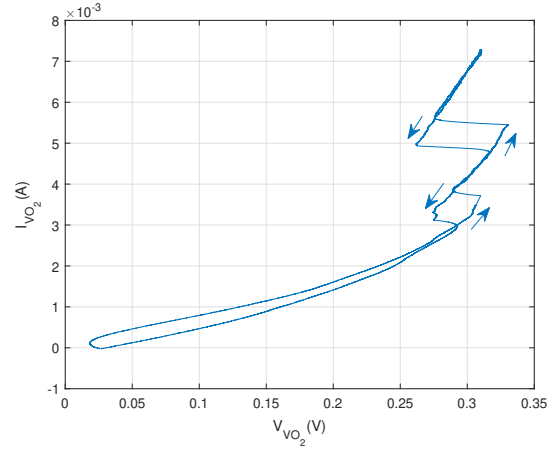
This effect of increase in the width of the hysteresis has actually been reported previously in literature [18]. Here we are able to show that this is not necessarily the case, and that a grain can hold a relatively low hysteresis width, further study of this grains is necessary to asses if further decreasing of the width is possible.

We tried one small test in the wide hysteresis bubble to see if this could be caused by the joule heating due to the applied current. We did a full temperature sweep (forward and backward) at a constant current of 1  $\mu$ A (blue curve shown in figure 45), then we did a forward temperature sweep at 1  $\mu$ A followed by a backward temperature sweep at 20  $\mu$  A. The idea was to try to see if joule heating could be playing a role in this bubble. In the end we expected to have an even wider hysteresis but the fact that the resulting curve with this second temperature sweep was the same as the one showed in figure 45 leaves us with many questions which should be explored further.

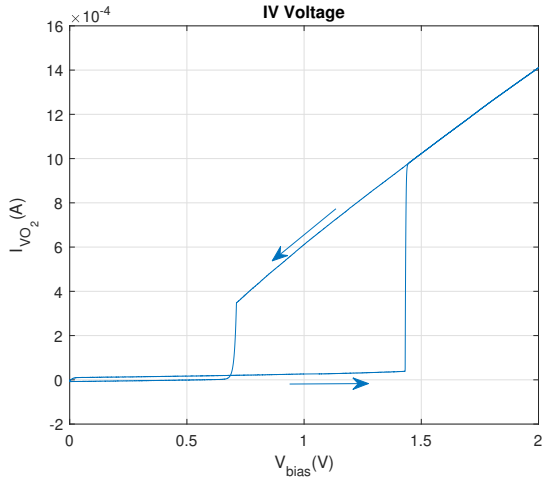
We were not able to continue the study of this nanoparticles since subsequently after their thermal characterisation they were tried with a current source to activate their phase change, but they burned. It was therefore decided that the IV characteristics of this bubbles would be done with voltage activation using the circuit shown in figure 6. Through this voltage activation we obtained the following IV characteristics on two other different devices:



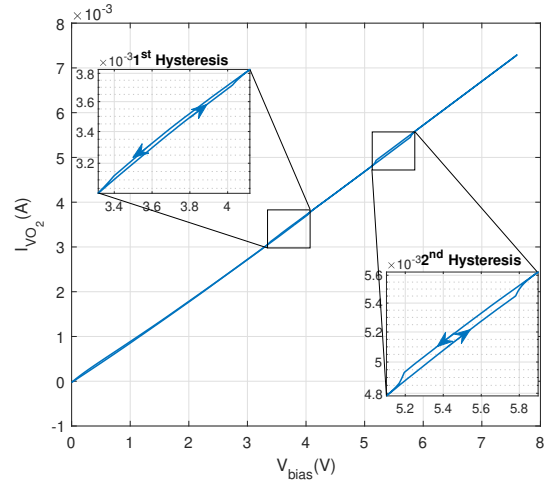
(a) Grain A IV.



(b) Grain B IV.



(c) Grain A, current vs applied voltage.



(d) Grain B, current vs applied voltage.

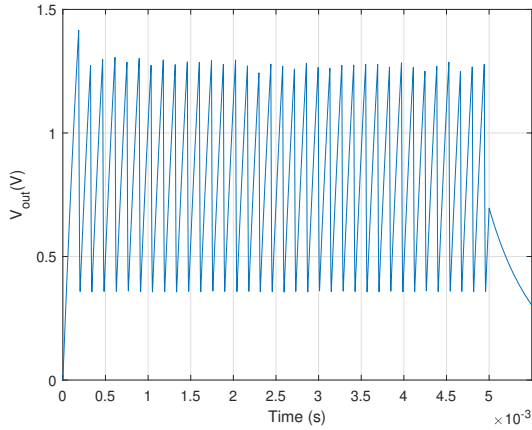
Figure 46: I-V characteristic and  $I - V_{bias}$  characteristic of two different grains, grain A and B

Above we show the different electrical characterizations of two different grains labeled A and B. The grain A is probably alone between the contacts and shows a perfect hysteresis, whereas grain B or more accurately the device B shows two different hysteresis probably belonging to two different grains that were contacted.

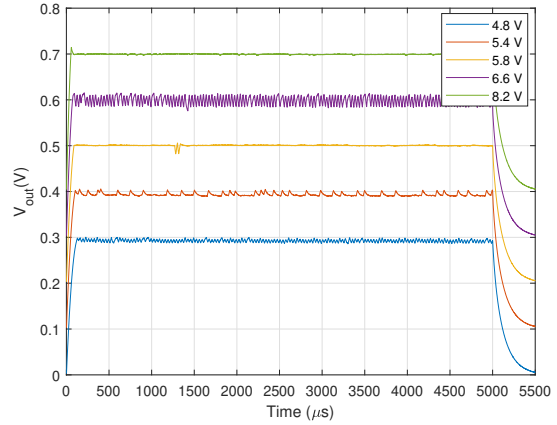
Thanks to these two characteristics one can see the difference between a single grain and a set of grains. Indeed for the IV characteristics one can see the difference between the bias needed to have the MIT, which is much more important in the set of grains, and therefore more power is needed for a multiple grain device than for an individual grain.

This shows how disadvantageous a single extra grain can be for these oscillators which would suggest that the fabrication of singular grain devices would be ideal.

Furthermore in the second system two regimes of oscillations can be found at different applied voltages as can be seen in figure 47b. And for the grain A the oscillations are very much near perfect, which further shows how ideal it would be to use this kind of device.



(a) Grain A Oscillations.



(b) Grain B Oscillations comparison with different bias voltage.

Figure 47: Comparison of oscillations for the two different devices

Finally we can say that the electrical results are consistent with what was previously seen in the Raman spectra, namely that the granular material is of higher quality than the smooth material. This is seen through their perfect hysteresis both in temperature and electrical activation. To understand exactly how this phase change works in these small bubbles much more research should be done to be able to harness their power for the fabrication of reliable oscillators.

Nevertheless the usage of this grains for the fabrication of oscillators can be an interesting path to take given the thermal and electrical characteristics shown before. And given the results of the previous section we should be able to fabricate these granular devices with the FA technique.

### 5.3 Conclusion

In this section we were able to characterize  $VO_2$  devices mainly on the crossbar or single grain configurations. We were not able to characterize any planar device in a significant and conclusive way.

Given that a crossbar device is closer to a single grain device than to a planar device (as shown in the small crossbar devices), the main take from these experiments is that in the CMOS compatibility framework the tendency for these devices should be to move close to singular grain devices as much as possible. This is consistent with the many Raman results obtained in the study of the thin films since the granular material shows consistently higher Raman peaks than the smooth films, which could signify higher quality of the material.

## 6 Simulation and Models

In the frame of the experimental work conducted on this thesis, films and devices with different granularity were characterized. From very smooth films, to granular films, to the contacting of a single grain device, the electrical activation of the phase change gave very different results, suggesting the high impact that the granularity has on the properties of the devices. For example, more than once in experiment was reported an IV characteristic underlying multiple phase-change steps, that we associate with different grain switching from insulating to metallic in the same device. To better understand how the phase change propagates in a single, multi-grain device and how other properties impact the oscillator performances, we have developed a simulation model of the devices, that is detailed in this chapter.

### 6.0.1 Conduction Model: Smooth Films

For a thin film of vanadium dioxide it has been reported hysteresis curves as the ones that were obtained in the first section of this thesis, and an effective model has been proposed to explain this smooth transition behaviour where there is a coexistence between metallic and insulating states [43, 40]. In such a model far below the IMT temperature the resistivity of the film is governed by an insulating state, which follows a thermal promotion of carriers law:

$$\rho = \rho_0 e^{\frac{E_a}{k_b T}} \quad (3)$$

where  $\rho$  is the resistivity of the material,  $\rho_0$  is a constant that represents the resistivity of the material at infinite temperature,  $E_a$  is the activation energy,  $k_b$  is Boltzman's constant and of course T is the temperature in Kelvin.

Then at relatively high temperatures the resistivity of the material is governed by a metallic state therefore follows a linear law with temperature:

$$\rho = \alpha T + \rho_1 \quad (4)$$

where alpha is a constant, T is temperature in Kelvin and  $\rho_1$  is the remnant resistance at low temperatures.

The extraction of the constants in this model can be done easily by looking at the variation of resistivity in low temperatures then in high temperatures, this task has been done for one of each of the kinds samples that were studied in the thin film section. The extrapolated values are found below:

Name	ALD 26nm FA(90,310,20)	ALD 46 nm FA(90,327,30)	PLD 50 nm Ge-doped FA(90,400,2)
$E_a$ (eV)	0.285	0.260	0.285
$\rho_0$ ( $\mu\Omega$ *cm)	219	368	245
$\alpha$ (m $\Omega$ *cm/K)	-5.87	-3.20	-0.470
$\rho_1$ ( $\Omega$ *cm)	2.36	1.33	0.198

Table 1: Extracted values form three different samples

This values seem to be in good accordance with what can be found in literature [43, 44, 45], with the activation energy being below the bulk  $VO_2$  previously measured value ( 0.4 eV) [45] but above other values found in single crystalline  $VO_2$  thin films [43].

These two extrapolation give a relatively good approximation of the two extreme behaviors of the material given by the two well known states of  $VO_2$ . Nevertheless the transition between the two is a bit harder to understand due to the high number of parameters that may come in place. The fundamental mechanism that takes the material from one state to the other is still not yet understood to begin with, however one can think of an comprehensive effective model of domain expansion like the ones used for ferromagnetic materials. In such a model at low temperature the film can be seen as a single insulating domain, with increasing temperature the resistivity of the film is governed by such a domain, then when we get closer to the transition temperature metallic domains start to appear because the nanocrystals (infinitesimal domains) composing the domain start to turn. Given that the transition here is solely temperature dependent all nanocrystals will transition independently from one another. Effectively we will have that a certain proportion of the material will become metallic until the metallic domain is more abundant than the insulating one. Given the nature of the measurement where we have two tips touching the sample, some papers argue that a percolative model [41] of current actually governs this measurement, since there is no need for the whole film to switch to metallic state for the tips to "see" a metallic resistance but it is only necessary that a certain portion of it connecting the two tips turns

to the metallic state so it dominates the measurement. Some other publications that have tried different models backup the idea that this percolative model is the better suited to explain this situation [46]. Now for us to be able to backup this behaviour some optical measurements could be done to see in absolute values the quantity of material that has turned at a certain temperature, this is possible because the transmittance of vanadium oxide is also dependent from temperature as resistivity.

### 6.0.2 Simulation: Granular Devices

In this section of the thesis we will go through the explanation and the results of the development of a toy model that was made to try to better understand our devices. As explained in the introduction of this thesis many have reported that a self joule heating effect can be one of the main transition causes of a voltage/current activated device. We will suppose for this part of the thesis that this is true. Therefore in our simulation the transition is caused only by temperature.

A very simplistic macroscopical model that captures the granularity of the material is the random resistor network model [40]. It consists of a network of resistors, where a group of four resistors connected at the same node represent a single grain (or a group of three if the grain is on the border of the device). The value of the resistors are initialized at random values following a Gaussian distribution, the average value was taken from our single bubble measurements in the device section. The IMT temperature for each grain is supposed to follow a Gaussian distribution with average value being  $64^{\circ}C$ . The four (or three) resistors of a same grain are supposed to have the same value. The point of the simulation is to apply a voltage or a current through the whole network, solve the voltages in each node inside of the network knowing the source voltage or current. Then we solve the thermal equation for each node given the voltages, we consider thermal conduction in between grains, thermal conduction between the grains and the pads, and the substrate and finally we consider self heating inside of each grain. The thermal model is set to "relax" until it reaches a certain steady-state, then for each grain the value of their resistance is updated according to their actual temperature. Then we do this again for an increasing/decreasing current, solving for each node and repeating the thermal calculation at each source value. A scheme of the network is shown in figure 8b.

A whole net is equivalent to a single planar device. Each grain is considered to act as a single "perfect" crystal where the temperature dependent hysteresis jump is a clear cut hysteresis as shown in figure 48, supposing that each grain is ideal.

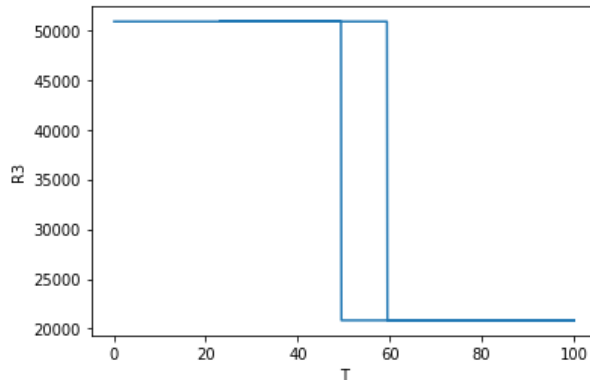


Figure 48: Single grain hysteresis used for our model, each grain has such a temperature characteristic in our simulation.

The choice of the source is also important. If we choose to use a current source, which was our case since we were trying to simulate our measurements. For each grain we would need to apply Kirchoff's law, conservation of current.

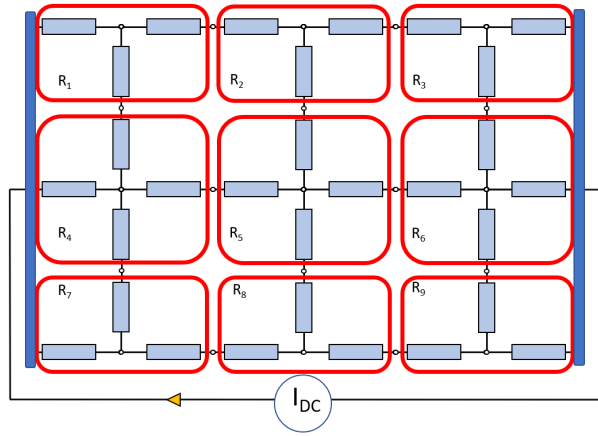


Figure 49: Scheme of a network of grains, each grain is delimited with a read line, inside we can see the resistors that make up each grain, each with the same value of resistance.

Given that our experiments with the devices used current as a source we will do the same in the simulations. To solve the electrical model, i.e. to find the voltages at each node we need to solve Kirchoff Law at each node. Below we put a scheme of the electrical model of each node.

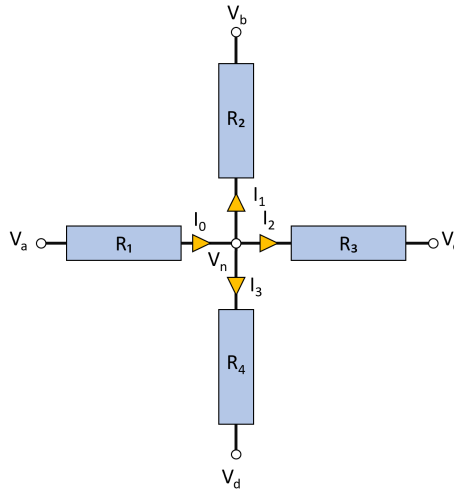


Figure 50: Electrical model of a single grain.

For the node shown above we have:

$$i_0 - i_1 - i_2 - i_3 = 0 \quad (5)$$

And thanks to Ohm's law this becomes:

$$\frac{V_a - V_n}{R_1} - \frac{V_n - V_b}{R_2} - \frac{V_n - V_c}{R_3} - \frac{V_n - V_d}{R_4} = 0 \quad (6)$$

This equation can be applied to each node (i.e. each grain) of the net, plus the equation corresponding to the node where the source current is divided into each branch. For each node we will have an equation and knowing that each node represents an unknown then the system happens to be a solvable system of  $N+1$  nodes with  $N+1$  equations (taking into account the source node at the left hand of the device scheme). This in python will be represented using matricial calculations. Where we will basically have Ohm's law in the form of matrices as follows:

$$\begin{bmatrix} \dots & \dots & \dots \\ \dots & R^{-1} & \dots \\ \dots & \dots & \dots \end{bmatrix} * \begin{bmatrix} V_0 \\ V_1 \\ V_2 \\ \vdots \\ \vdots \\ \vdots \end{bmatrix} = \begin{bmatrix} I_{dc} \\ 0 \\ 0 \\ \vdots \\ \vdots \\ \vdots \end{bmatrix} \quad (7)$$

The system is solved by python, and from this we retrieve the potentials vector which we then use to solve the thermal equation:

$$\rho C_p \frac{\partial T}{\partial t} = k \nabla^2 T + Q \quad (8)$$

Where T is the temperature, t is time,  $\rho$  is the density,  $C_p$  is the heat capacity, k is the thermal conductivity and Q is the dissipated heat of the concerned grain.

In this equation we have that the variation of temperature in time is equal to the heat exchange between the considered bodies, in this case it consists of the heat exchange between one grain and its neighbours, in the horizontal plain, and vertically with the substrate or the two pads depending on which device configuration we are considering. The last term Q is, in our situation, the heat produced by Joule effect in the grain in consideration.

If we assume that the temperature is homogeneous inside of the grain we will have that in such a lumped model equation 8 's solution becomes:

$$T_i(t+1) = T_i(t) + \left( \frac{k_{g-g}}{\rho C_p} (T_{up} + T_{down} + T_{right} + T_{left} - 4T_i(t)) + \frac{P}{\rho C_p V} - \frac{k_{subs}(T_i(t) - T_R)}{\rho C_p t_k} \right) * \delta t \quad (9)$$

Where  $T_i(t)$  is the temperature of the  $i^{th}$  grain (counting from left to right and then from top to bottom) at the t time,  $\delta t$  is the time step or the time resolution,  $\rho$  is the density,  $C_p$  the heat capacitance,  $k_{g-g}$  is the thermal conductivity between two grains,  $k_{subs}$  is the thermal conductivity between the grains and the substrate, P is the joule dissipated power,  $t_k$  is the thickness of the grain and V is the volume of the grain.  $T_{up}$ ,  $T_{down}$ ,  $T_{left}$ ,  $T_{right}$  are the temperatures of neighbours of the considered grains. And finally  $T_R$  is room temperature considered to be  $23^\circ C$ . The last term of the equation 9 is actually the heat dissipation that goes to the pads or to the substrate which are considered to be perfect heat sinks.

Similar models have been used a few times before to capture the properties of  $VO_2$  based devices, showing similar experimental results to ours [40, 41, 42].

Since our planar devices didn't work we decided to simulate the ones that did work to compare results. The model being for planar devices, some slight modifications had to be done. For the crossbar model, first one has to think about the fact that the current is applied vertically, supposing that between the pads there is only one layer of grains we can keep the network but we have to add "vertical" resistances that are connected to both pads, this ones are represented by the green resistors added in the initial network scheme (see figure 51). The thermal model is kept the same.

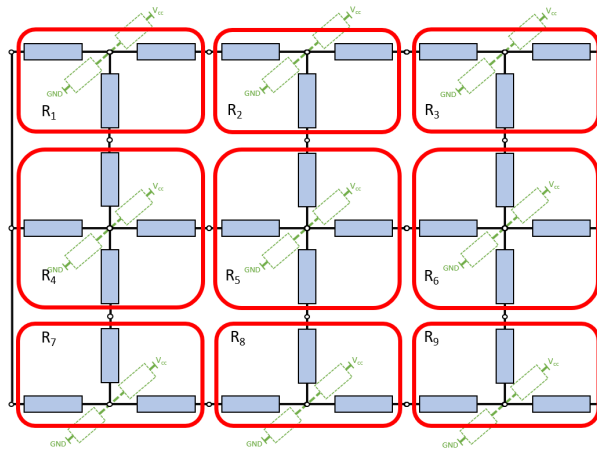


Figure 51: Electrical model of crossbar.

Such a change just adds extra terms in the resistance matrix, the calculations are exactly the same.

After a few initial trials with such a model it was realized that the calculated intergranular/horizontal current was basically null, so an extra simplification of this model could be made. The final electrical model was simply a set of parallel resistors that changed with temperature with a steep hysteresis, so the thermal model is key in this simulation. Despite the simplistic nature of this model the results are surprisingly close to what we obtained previously with both current (see figure 53) and temperature sweeps. With a 4x4 matrix network and with a 10x10 we obtain the results below.

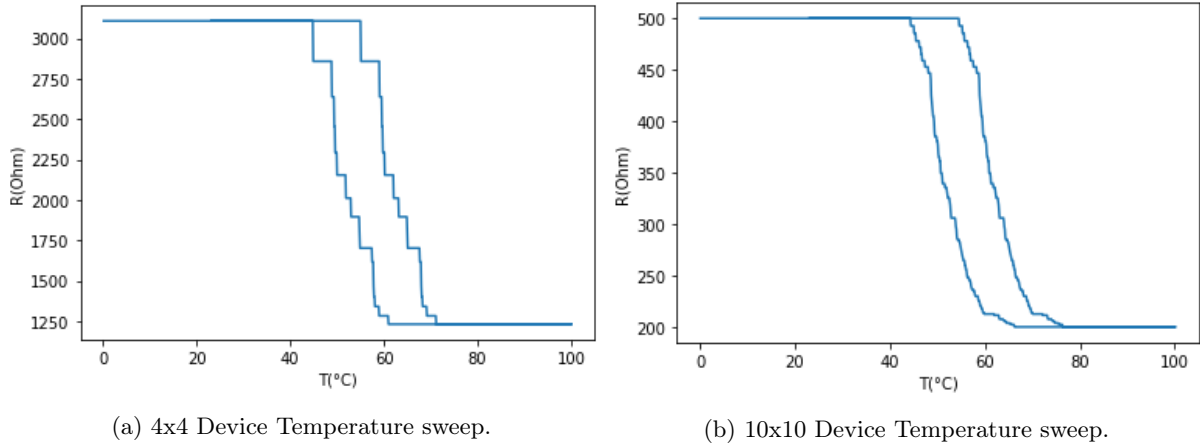


Figure 52: Temperature sweeps for two different kinds of devices.

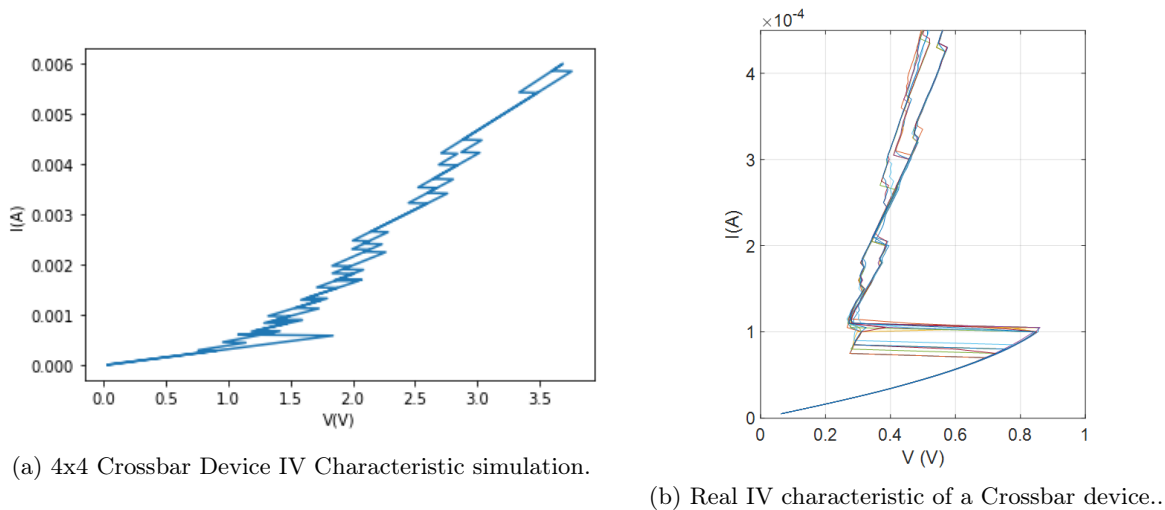


Figure 53: Comparison with Simulated and Real IV characteristic of a Crossbar device.

Our simulation results are qualitatively comparable to what we have, this being said, quantitatively the model is probably too simple to compare. Nevertheless having such similar results with such a simple code leaves ground to a lot of possibilities. Indeed the choice of going from the network to the parallel resistors was done to lower the complexity of the calculations, now the electrical model is so simple in terms of complexity one can play much more with the randomness that is allowed to each parameter of the simulation. For example in this instance we have just put randomness in the initial value of the resistors at room temperature (i.e. their insulating value) and for the IMT temperature but one can also add randomness in the metallic value, in the width of the hysteresis, etc... One can also think of a more complex thermal model that do not considers that the temperature is homogeneous in the grains.

But in here we can say with a certain degree of confidence that our devices actually act as a set of almost independent domains that themselves act as individual grains with possibly near perfect monocry-stalline  $VO_2$  characteristics, and that the main actuator within the devices is heat.

Another point that this simulation clarifies is how the two sweeps (or two activations) actually make the device behave so differently. As proposed before, the temperature sweep will simply "activate" each domain separately once their respective IMT temperature is reached, whereas in the current activation

it depends on the initial conditions, specifically on the initial value of each resistor, since for low currents there will be preferential paths, where the current will mostly flow on the least resistive path, and therefore heat this specific path more than the others making it reach its transition point first which can be related to the initial jump which is the most important one always, then surrounding domains will be more susceptible to be activated more promptly in the sweep but given the effective state of the whole device the jumps are smaller and smaller. In a certain way the crossbar configuration is very close to a singular domain device for the IV characteristics, since the first domain to switch is effectively a stand alone grain. In any case this simulation shows very well the fact that the granularity of the device adds many degrees of freedom on the whole system and this model should be explored further with a more complete model.

## 7 Conclusion

The  $VO_2$  compound is a material with high potential for the fabrication of physical neural networks, using it to make oscillators.

We explored the different phenomena that affects the fabrication of oscillators from this material in a CMOS-compatible context.

Our choices were met with many challenges but we were able to achieve our main goals.

This thesis focused on optimizing an ALD deposition process for  $VO_2$  using TEMAV for Vanadium, and exploring three different precursors for oxygen. We were able to conclude that water gives the best results in terms of reproducibility of the material qualities.

For the annealing technique, we investigated a previously unexplored technique, the flash anneal. With this kind of anneal we were able to characterize the different phases the oxide goes through in the annealing process, in accordance with what was found previously by researchers using common annealing methods. The material goes from the amorphous deposited form into a smooth  $VO_2$ , with low quality of crystals. With higher applied energy through the form of thermal energy or radiation energy the material becomes more granular and becomes of higher quality. With even higher energy the material starts to become  $V_2O_5$ ,  $VO_2$ 's more stable counterpart. As in the scope of this research, I was able to demonstrate that the flash anneal process can help to achieve very smooth films with limited grain-size dimensions. However, further development of these films into devices has proven difficult. This led to the conclusion that very granular films holds better phase-change properties and therefore allow to achieve better performing device. The ultimate limit is the fabrication of a device on a single  $VO_2$  grain, which was also demonstrated in Chapter 8 of this thesis. This architecture posses a lot of extra obstacles. For example, since the position where the grains appear is random in the chip it causes that the design of the contacts has to be changed for each new chip. One possible solution for this is to do the deposition of the material only in small sections of the chip and then recur to the anneal, therefore limiting spatially the appearance of the grains. But then we would have to change the conditions of the anneal, and therefore this should be explored in the future research activities.

As a side result, we investigated the capabilities of the flash anneal technique to trim the transition temperature of Ge-doped  $VO_2$  samples, and we concluded we were able to push the IMT from  $65^\circ C$  to around  $70^\circ C$ .

We explored the fabrication of devices to discern which architecture was the best suited for our purposes. We found that devices fabricated in crossbar configuration are in general more reliable and closer to an ideal single-grain operation.

We finally tried to explain how the electrical conduction happened in this devices. We were able to learn that due to the granularity of the material extra phenomena would act in addition to the mechanisms that already act in a monocrystal material. In the end the fact that we work in Si substrates adds many difficulties to the development of this technologies but we were able to surpass this difficulties, and therefore the added value of using such substrates is not lost.

However much remains to be done. For the process of fabrication we were not able to optimize at the best of our capabilities the annealing conditions such as to get the best crystals. Much could have been done to correlate the average size of the grains with the annealing conditions, and with the electrical characterization.

Finally, we modelled our devices to achieve better understanding on the electrically-driven phase change, in which we could observe how multiple grain switching can affect the device performances. A more precise model could be used to give more insight, for example exploring a nucleation model for phase-change domains.

As a conclusion, even though we were not able to answer all the questions regarding the fabrication of this material on Si, this thesis offered a step forward for the research team in IBM to develop a potential new product.

## References

- [1] Izhikevich E. Computing with oscillators. *Neural Networks* 2000;5255:1–30.
- [2] Raychowdhury A, et al. Computing with networks of oscillatory dynamical systems. *Proc IEEE* 2019;107(1):73–89.
- [3] Shukla N, et al. Synchronized charge oscillations in correlated electron systems. *Sci Rep* 2015;4(1):4964
- [4] Wunderlich T, Kungl A. F., Müller E., Hartel A., Stradmann Y., Aamir S. A., Grübl A., Heimbrecht A., Schreiber K., Stöckel D., Pehle C., Billaudelle S., Kiene G., Mauch C., Schemmel J., Meier K., Petrovici M. A., "Demonstrating Advantages of Neuromorphic Computation: A Pilot Study" , *Front. Neurosci.*, 26 March 2019.
- [5] Z. Yang, C. Ko, S. Ramanathan, "Oxide Electronics Utilizing Ultrafast Metal-Insulator Transitions", *Annu. Rev. Mater. Res.*41:337–67, 2011.
- [6] Pergament, Alexander, Aurelian Crunteanu, Arnaud Beaumont, Genrikh Stefanovich and Andrey Velichko. "Vanadium Dioxide: Metal-Insulator Transition, Electrical Switching and Oscillations. A Review of State of the Art and Recent Progress." (2015).
- [7] J. Leroy, A. Cruteanu, A. Bessaudou, F. Cosset, C. Champeaux, and J.-C. Orlianges, "High-speed metal-insulator transition in vanadium dioxide films induced by an electrical pulsed voltage over nano-gap electrodes," *Appl. Phys. Lett.*, vol.100,no.21,p.213507,2012.
- [8] Wegkamp, Daniel, and Julia Stähler. "Ultrafast Dynamics during the Photoinduced Phase Transition in VO<sub>2</sub>." *Progress in Surface Science* 90, no. 4 (December 1, 2015): 464–502.
- [9] S.V.Strelstov, D.I.Khomskii, "Orbital Physics in transition metal compounds:new trends", *Uspekhi Fizicheskikh Nauk (UFN) Journal*, 2017.
- [10] Goodenough J.B., "The Two Components of the Crystallographic Transition in VO<sub>2</sub>", *Journal of Solid State Chemistry* 3,490-500,1971.
- [11] Wentzcovitch, R.M., Schulz, W.W., Allen, P.B. "VO<sub>2</sub>: Peierls or Mott-Hubbard? A view from band theory." *Phys. Rev. Lett.* 72,3389, 1994.
- [12] Liebsch, A., Ishida, H. and Bihlmayer, G. "Coulomb correlations and orbital polarization in the metal-insulator transition of VO<sub>2</sub>." *Phys. Rev. B* 71,085109, 2005.
- [13] Shao, Zewei, Xun Cao, Hongjie Luo, and Ping Jin. "Recent Progress in the Phase-Transition Mechanism and Modulation of Vanadium Dioxide Materials." *NPG Asia Materials* 10, no. 7 (July 2018): 581–605.
- [14] F. J. Morin, "Oxides which show a metal-to-insulator transition at the Neel temperature", *Phys. Rev. Lett.*, vol. 3,no. 34, 1959.
- [15] Paul W. *Mater. Res. Bull.* 5, 691, 1970.
- [16] Pauli, S. A., R. Herger, P. R. Willmott, E. U. Donev, J. Y. Suh, and R. F. Haglund. "X-Ray Diffraction Studies of the Growth of Vanadium Dioxide Nanoparticles." *Journal of Applied Physics* 102, no. 7 (October 2007): 073527.
- [17] Krammer, Anna, Arnaud Magrez, Wolfgang A. Vitale, Piotr Mocny, Patrick Jeanneret, Edouard Guibert, Harry J. Whitlow, Adrian M. Ionescu, and Andreas Schüler. "Elevated Transition Temperature in Ge Doped VO<sub>2</sub> Thin Films." *Journal of Applied Physics* 122, no. 4 (July 28, 2017)
- [18] Suh, J. Y., R. Lopez, L. C. Feldman, and R. F. Haglund. "Semiconductor to Metal Phase Transition in the Nucleation and Growth of VO<sub>2</sub> Nanoparticles and Thin Films." *Journal of Applied Physics* 96, no. 2 (July 15, 2004): 1209–13.

- [19] E. Corti, B. Gotsmann, K. Moselund, I. Stolichnov, A. Ionescu and S. Karg, "Resistive Coupled VO<sub>2</sub> Oscillators for Image Recognition", 2018 IEEE International Conference on Rebooting Computing (ICRC), McLean, VA, USA, 2018, pp. 1-7.
- [20] Brassard, D., S. Fourmaux, M. Jean-Jacques, J. C. Kieffer, and M. A. El Khakani. "Grain Size Effect on the Semiconductor-Metal Phase Transition Characteristics of Magnetron-Sputtered VO<sub>2</sub> Thin Films." *Applied Physics Letters* 87, no. 5 (August 2005): 051910.
- [21] E. Corti, B. Gotsmann, K. Moselund, A. Ionescu, J. Robertson and S. Karg, "Scaled resistively-coupled VO<sub>2</sub> oscillators for neuromorphic computing", *Solid-State Electronics*, Volume 168, 2020, 107729, ISSN 0038-1101.
- [22] S. Datta, N. Shukla, M. Cotter, A. Parihar and A. Raychowdhury, "Neuro inspired computing with coupled relaxation oscillators," 2014 51st ACM/EDAC/IEEE Design Automation Conference (DAC), San Francisco, CA, 2014, pp. 1-6, doi: 10.1145/2593069.2596685.
- [23] A. Beaumont, J. Leroy, J.-C. Orlianges, and A. Crunteanu, "Current-induced electrical self-oscillations across out-of-plane threshold switches based on VO<sub>2</sub> layers integrated in crossbars geometry", *J. Appl. Phys.* 114, 244301, 2013
- [24] Peter, Antony P., Koen Martens, Geert Rampelberg, Michael Toeller, James M. Ablett, Johan Meersschaut, Daniel Cuypers, et al. "Metal-Insulator Transition in ALD VO<sub>2</sub> Ultrathin Films and Nanoparticles: Morphological Control." *Advanced Functional Materials* 25, no. 5 (February 2015): 679–86.
- [25] Liao, G. M., S. Chen, L. L. Fan, Y. L. Chen, X. Q. Wang, H. Ren, Z. M. Zhang, and C. W. Zou. "Dynamically Tracking the Joule Heating Effect on the Voltage Induced Metal-Insulator Transition in VO<sub>2</sub> Crystal Film." *AIP Advances* 6, no. 4 (April 2016): 045014.
- [26] Singh, Sujay, Gregory Horrocks, Peter M. Marley, Zhenzhong Shi, Sarbajit Banerjee, and G. Sambandamurthy. "Proliferation of Metallic Domains Caused by Inhomogeneous Heating near the Electrically Driven Transition in VO<sub>2</sub> Nanobeams." *Physical Review B* 92, no. 15 (October 12, 2015): 155121.
- [27] Simon Mun, Bongjin, Joonseok Yoon, Sung-Kwan Mo, Kai Chen, Nobumichi Tamura, Catherine Dejoie, Martin Kunz, et al. "Role of Joule Heating Effect and Bulk-Surface Phases in Voltage-Driven Metal-Insulator Transition in VO<sub>2</sub> Crystal." *Applied Physics Letters* 103, no. 6 (August 5, 2013): 061902.
- [28] Y. Muraoka and Z. Hiroi, "Metal-insulator transition of VO<sub>2</sub> thin films grown on TiO<sub>2</sub>(001) and (110) substrates.", *Applied Physics Letters* 80:4, 583-585, 2002.
- [29] Y. Zhou and S. Ramanathan, "Heteroepitaxial VO<sub>2</sub> thin films on GaN: Structure and metal-insulator transition characteristics.", *Journal of Applied Physics* 112:7, 074114, 2012.
- [30] Kozen, Alexander C., Howie Jores, Marc Currie, Virginia R. Anderson, Charles R. Eddy, and Virginia D. Wheeler. "Structural Characterization of Atomic Layer Deposited Vanadium Dioxide." *The Journal of Physical Chemistry C* 121, no. 35 (September 7, 2017): 19341–47.
- [31] P. A. Premkumar, M. Toeller, I. P. Radu, C. Adelman, M. Schaekers, J. Meersschaut, T. Conard and S. V. Elshocht, "Process Study and Characterization of VO<sub>2</sub> Thin Films Synthesized by ALD Using TEMAV and O<sub>3</sub> Precursors", *ECS J. Solid State Sci. Technol.* 2012, Volume 1, Issue 4, Pages P169-P174.
- [32] K. Zhang, M. Tangirala, D. Nminibapiel, W. Cao, V. Pallem, C. Dussarrat and H. Baumgart, "Synthesis of VO<sub>2</sub> Thin Films by Atomic Layer Deposition with TEMAV as Precursor", *ECS Transactions* ,50(13):175-182, 2013
- [33] Zhang, Chunzi, Qiaoqin Yang, Cyril Koughia, Fan Ye, Mohsen Sanayei, Shi-Jie Wen, and Safa Kasap. "Characterization of Vanadium Oxide Thin Films with Different Stoichiometry Using Raman Spectroscopy." *Thin Solid Films* 620 (December 1, 2016): 64–69. <https://doi.org/10.1016/j.tsf.2016.07.082>.

- [34] Rebohle, Lars, Slawomir Prucnal, and Denise Reichel. *Flash Lamp Annealing: From Basics to Applications*. Vol. 288. Springer Series in Materials Science. Cham: Springer International Publishing, 2019.
- [35] O'Connor, Éamon, Mattia Halter, Felix Eltes, Marilyne Sousa, Andrew Kellock, Stefan Abel, and Jean Fompeyrine. "Stabilization of Ferroelectric Hf x Zr 1x O 2 Films Using a Millisecond Flash Lamp Annealing Technique." *APL Materials* 6, no. 12 (December 2018): 121103.
- [36] Liu, Yueyan, Juncheng Liu, Yuanbao Li, Danping Wang, Lin Ren, and Kaishun Zou. "Effect of Annealing Temperature on the Structure and Properties of Vanadium Oxide Films." *Optical Materials Express* 6, no. 5 (May 1, 2016): 1552.
- [37] Parker, J. C. "Raman Scattering from VO 2 Single Crystals: A Study of the Effects of Surface Oxidation." *Physical Review B* 42, no. 5 (August 15, 1990): 3164–66.
- [38] Lust, Mark, Shangyi Chen, Catrina E. Wilson, Joshua Argo, Vicky Doan-Nguyen, and Nima Ghalichechian. "High-Contrast, Highly Textured VO 2 Thin Films Integrated on Silicon Substrates Using Annealed Al 2 O 3 Buffer Layers." *Journal of Applied Physics* 127, no. 20 (May 29, 2020): 205303. <https://doi.org/10.1063/1.5144816>.
- [39] Menges, Fabian, Philipp Mensch, Heinz Schmid, Heike Riel, Andreas Stemmer, and Bernd Gotsmann. "Temperature Mapping of Operating Nanoscale Devices by Scanning Probe Thermometry." *Nature Communications* 7, no. 1 (April 2016): 10874.
- [40] Wang, Xingzhi. "Modeling of Temperature-Dependent Resistance in Micro- and Nanopolycrystalline VO2 Thin Films with Random Resistor Networks." *Optical Engineering* 47, no. 3 (March 1, 2008): 033801. <https://doi.org/10.1117/1.2894146>.
- [41] Rozen, John, René Lopez, Richard F. Haglund, and Leonard C. Feldman. "Two-Dimensional Current Percolation in Nanocrystalline Vanadiumdioxide Films." *Applied Physics Letters* 88, no. 8 (February 20, 2006): 081902. <https://doi.org/10.1063/1.2175490>.
- [42] Takami, Hidefumi, Teruo Kanki, and Hidekazu Tanaka. "Multistep Metal Insulator Transition in VO 2 Nanowires on Al 2 O 3 (0001) Substrates." *Applied Physics Letters* 104, no. 2 (January 13, 2014): 023104. <https://doi.org/10.1063/1.4861720>.
- [43] Zhong, Xing, Xueyu Zhang, Arunava Gupta, and P. LeClair. "Avalanche Breakdown in Microscale VO 2 Structures." *Journal of Applied Physics* 110, no. 8 (October 15, 2011): 084516. <https://doi.org/10.1063/1.3654121>.
- [44] Cao, J., W. Fan, K. Chen, N. Tamura, M. Kunz, V. Eyert, and J. Wu. "Constant Threshold Resistivity in the Metal-Insulator Transition of VO 2." *Physical Review B* 82, no. 24 (December 7, 2010): 241101. <https://doi.org/10.1103/PhysRevB.82.241101>.
- [45] Rosevear, W. H., and W. Paul. "Hall Effect in VO<sub>2</sub> near the Semiconductor-to-Metal Transition." *Physical Review B* 7, no. 5 (March 1, 1973): 2109–11. <https://doi.org/10.1103/PhysRevB.7.2109>.
- [46] Annasiwatta, Chandika, Jinhao Chen, Jordan M. Berg, Ayrton Bernussi, Zhaoyang Fan, and Beibei Ren. "Multi-Physics Modeling of Hysteresis in Vanadium Dioxide Thin Films." In *2016 American Control Conference (ACC)*, 6905–10. Boston, MA, USA: IEEE, 2016. <https://doi.org/10.1109/ACC.2016.7526760>.